The Use of Alkali Activated Materials in Nuclear Industry

Peer-reviewed author version

MAST, Bram; SCHROEYERS, Wouter; Pontikes, Yiannis; VANDOREN, Bram & SCHREURS, Sonja (2020) The Use of Alkali Activated Materials in Nuclear Industry. In: Konings, Rudy (Ed.). Reference Module in Materials Science and Materials Engineering, Elsevier, p. 1-20.

DOI: 10.1016/B978-0-12-803581-8.11629-7
Handle: http://hdl.handle.net/1942/30631

Published in *Reference Module in Materials Science and Materials Egineering (2020)*
doi:10.1016/B978-0-12-803581-8.11629-7

Comprehensive Nuclear Materials – 2nd edition
Chapter 8. Spent fuel processing and waste disposal
00135 The use of alkali activated materials in nuclear industry

Bram Mast[a*], Wouter Schroeyers[a], Yiannis Pontikes[b], Bram Vandoren[c], Sonja Schreurs[a**]

[a] Hasselt University, CMK, NuTeC, Nuclear Technology - Faculty of Engineering Technology, Agoralaan Building H, B-3590 Diepenbeek, Belgium

[b] KU Leuven, Department of Materials Engineering, Kasteelpark Arenberg 44, 3001 Heverlee, Belgium

[c] Hasselt University, CERG, Faculty of Engineering Technology, Agoralaan Building H, B-3590 Diepenbeek, Belgium

[*] Main Author, E-mail: bram.mast@uhasselt.be

[**]Corresponding Author: sonja.schreurs@uhasselt.be

Abstract

Alkali Activated Materials (AAMs) are interesting alternative binder materials to Ordinary Portland Cement (OPC) for application in nuclear safety structures and radioactive waste management. AAMs are highly chemical and temperature resistant and can reach a high shielding capacity for gamma irradiation. AAMs also have a low calcium content which enables the addition of fluorine to reduce the H_2 production for Mg-containing wastes and limits the formation of ^{41}Ca due to neutron activation. In general, AAMs have lower radiolytic hydrogen yields compared to OPC.

Fayalite slag based AAMs were proven to have a similar gamma shielding capacity to basalt-magnetite concretes. Boron based AAMs form an interesting opportunity for neutron shielding. Since dehydration in AAMs is limited, better neutron shielding capacities for AAMs can be obtained compared to aged concrete.

The absence of portlandite, the low water content and the high alkalinity, make AAMs interesting candidates for the conditioning of certain radioactive waste streams. Ions as Cs^+ and Sr^{2+} can be incorporated in the AAM-gel or can be trapped in the self-generated or introduced zeolite structures in the AAM. Also, precipitation of several elements as a hydroxide can be promoted by selecting the right raw material and activation solution.

Keywords

- Alkali activated materials
- Geopolymers
- Shielding performance
- Stability under ionizing radiation
- Radiolytic hydrogen gas yield
- Radioactive waste conditioning materials

Published in *Reference Module in Materials Science and Materials Egineering (2020)*
doi:10.1016/B978-0-12-803581-8.11629-7

Abbreviations

μ	Linear attenuation coefficient
AAM	Alkali Activated Material
HDC	High Density Concrete
ILW	Intermediate-level radioactive waste
IP	Inorganic Polymer
LET	Linear energy transfer
LLW	Low-level radioactive waste
OPC	Ordinary Portland cement
PE	Polyethylene
PSD	Pore size distribution
RAW	Radioactive Waste

1. Introduction 3
2. Alkali Activated Materials as a shielding material 6
2.1. Shielding performance of AAMs 6
2.2. Effects on AAMs in a gamma irradiation field 8
2.3. Effects on AAMs in an electron irradiation field 14
2.4. Effects on AAMs in an alpha particle irradiation field 14
2.5. Effects on AAMs in a neutron irradiation field 15
3. Alkali Activated Materials as conditioning material 18
3.1. Liquid wastes 19
3.2. Zeolites 22
3.3. Aluminum containing waste 23
3.4. Mg alloys 23
3.5. An example 25
4. Conclusions and Outlook 26
References 27
Relevant Websites: 33

Published in *Reference Module in Materials Science and Materials Egineering (2020)*
doi:10.1016/B978-0-12-803581-8.11629-7

1. Introduction

For some decades, alternatives to the commonly used ordinary Portland cement (OPC) matrices are increasingly being studied. Alkali Activated Materials (AAMs) are one of the alternatives currently studied intensively due to their potential utilization as a high performance, environment friendly and sustainable alternative to Portland cement. This chapter will focus on the use of AAMs in nuclear applications with special attention to the effects of ionizing radiation on the matrix and to the immobilization mechanisms for the incorporated radionuclides.

Alkali activated materials encompass a broad range of binder systems formed by the reaction of an alkali metal source (solid or dissolved) with a solid powdered precursor[1]. The precursor can be a calcium silicate source comparable to the conventional clinkers, or an aluminosilicate source such as kaolinite, or fly ash; metallurgical slags, bottom ashes, tailings and other secondary resources are also explored as precursors but the specifics depend per case[1]. The alkali source can be any solid or solution which can raise the pH of the reaction mixture and dissolve the precursor[1]. A wide range of activating sources exists: alkali hydroxides, silicates, carbonates, sulphates, aluminates and oxides. As shown in Figure 1, the widely used term geopolymers in fact refers to a subclass of AAMs (although a general consensus has not been reached yet on the terminology). Geopolymers are highly coordinated binder systems which have a low calcium content and for which the network almost exclusively consists of aluminosilicate[1,2]. The network is built out of SiO_4 and AlO_4 tetrahedras linked by a sharing oxygen atom[2] (Figure 2). Another term often used is Inorganic Polymer (IP). IPs are 3D polymers made of inorganic elements bound in a connected network as a result of a polycondensation reaction for which the chemistry does not purely consist out of aluminiumsilicates. The term IP is in literature often used when a precursor is mixed with an alkali metal hydroxide or silicate to produce a binder, not matching the definition of a geopolymer. Since Ca and Al are not necessary for IP synthesis, this class is not included in Figure 1. Depending on the type of precursor material and the final network formed, also other terms can be found in literature: soil cements, geocements, alkaline cements, geoceramics and a variety of other names[1,3].

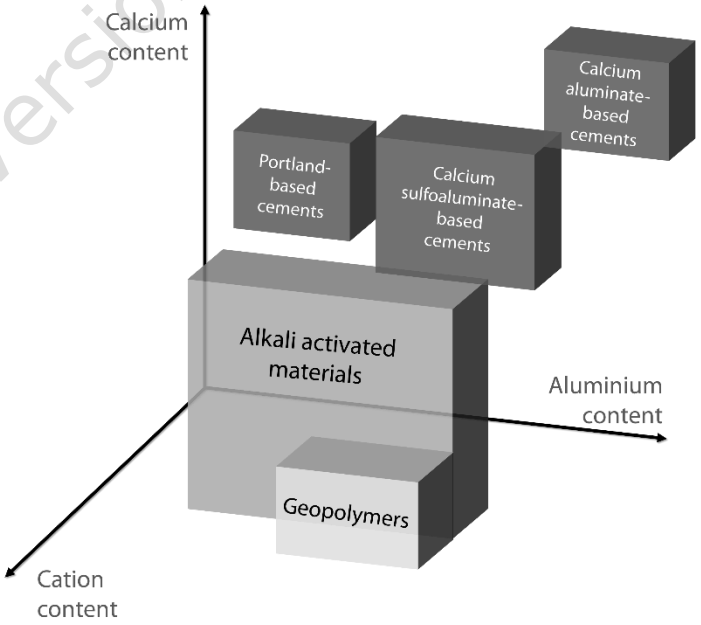

Figure 1: Schematic overview of alternative cements including AAM and geopolymers compared to Ordinary Portland cements, calcium sulfoaluminate cements and calcium aluminate cements reproduced with permission from Provis & Van Deventer (2014)[1].

The chemistry of alkali-activation can be summarized in four steps: (i) dissolution, (ii) reorganization, (iii) nucleation and (iv) polymerization and hardening[4] (Figure 3). In the first step, the ionic bonds (Ca-O) and covalent bonds (Si-O and Al-O) are broken at the surface of a precursor material in contact with a high alkaline solution. The alkaline cations (OH^-), present in the activator are good electron donor ions and act as a catalyst for breaking the covalent bonds in the aluminosilicate source. The dissolution occurs rapidly at high pH and consumes water. Because Al-O bonds are weaker than Si-O bonds, the initial gel will contain a higher amount of Al in comparison to Si. Next, the diffusion of the alkali solution will bring more Al^{3+} and Si^{4+} into solution. In the alkaline environment, the alumina and silica forms monomeric tetrahedral structures of $Al(OH)_4)^-$ and $Si(OH)_4$). Due to polycondensation reactions, the gel will harden with the formation of an amorphous 3D network of Al-O-Si chains. In this structure, each Al- and Si-atom is bonded to four oxygen atoms. The resulting negative charge is compensated by the anions present in the activation solution (e.g. Na^+, K^+, Li^+, Ca^{2+}, Ba^{2+}, NH_4^+, H_3O^+). Although the process is summarized in four steps, it should be mentioned that the different steps occur simultaneously[3,5]. At the end, a three-phase material is formed consisting out of pores, binder and aggregates of which the binder is reacted precursor material and the aggregates are unreacted precursor particles.

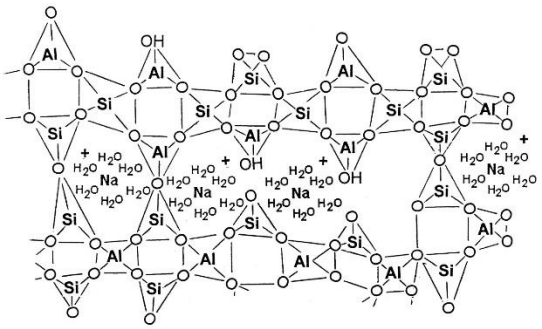

Figure 2: Schematic structure of a 3D Na-aluminosilicate network with Si-atoms bond to two or three Al-atoms with a sharing O-atom reproduced with permission from Barbosa et al. (2000)[6]. Not all Al is 4-fold coordinated in this figure as it would be the case for a geopolymer according to the definition of Davidovits[7].

The first three steps of alkali-activation are similar for all kind of systems. The last step, with the formation of the final structure, however highly depends on the calcium content of the reacting system as shown in Figure 3. It is important to make a division in two main groups according to the types of gel that dominates the structure. The primary reaction product can either be an alkali (sodium/potassium) aluminosilicate (N(-C)-A-S(-H)) or K(-C)-A-S(-H))[a]-type gel for low-Ca precursors or a calcium (sodium) (alumino)silicate hydrate (C(-N)(-A)-S-H)-type gel for a high-Ca precursor. For low-Ca binder systems, the 'H' is placed between parentheses to indicate that water is not a major structural component of the gel. Moreover, recent study of Peys et al.[8] indicated the participation of Fe in the silicate network which enables the use of Fe-rich precursors for AAM production. These precursors are slags, originating from nonferrous metallurgical industries which are currently underutilized. Fe-rich AAMs offer an interesting alternative to the high-density concretes (HDC) currently used as a gamma-ray shielding material[9].

[a] The chemical formulas are abbreviated to the oxide units. N represents Na_2O, K stands for K_2O, C for CaO, A for Al_2O_3, S for SiO_2, and H for H_2O. Minor or optional components are placed between parentheses.

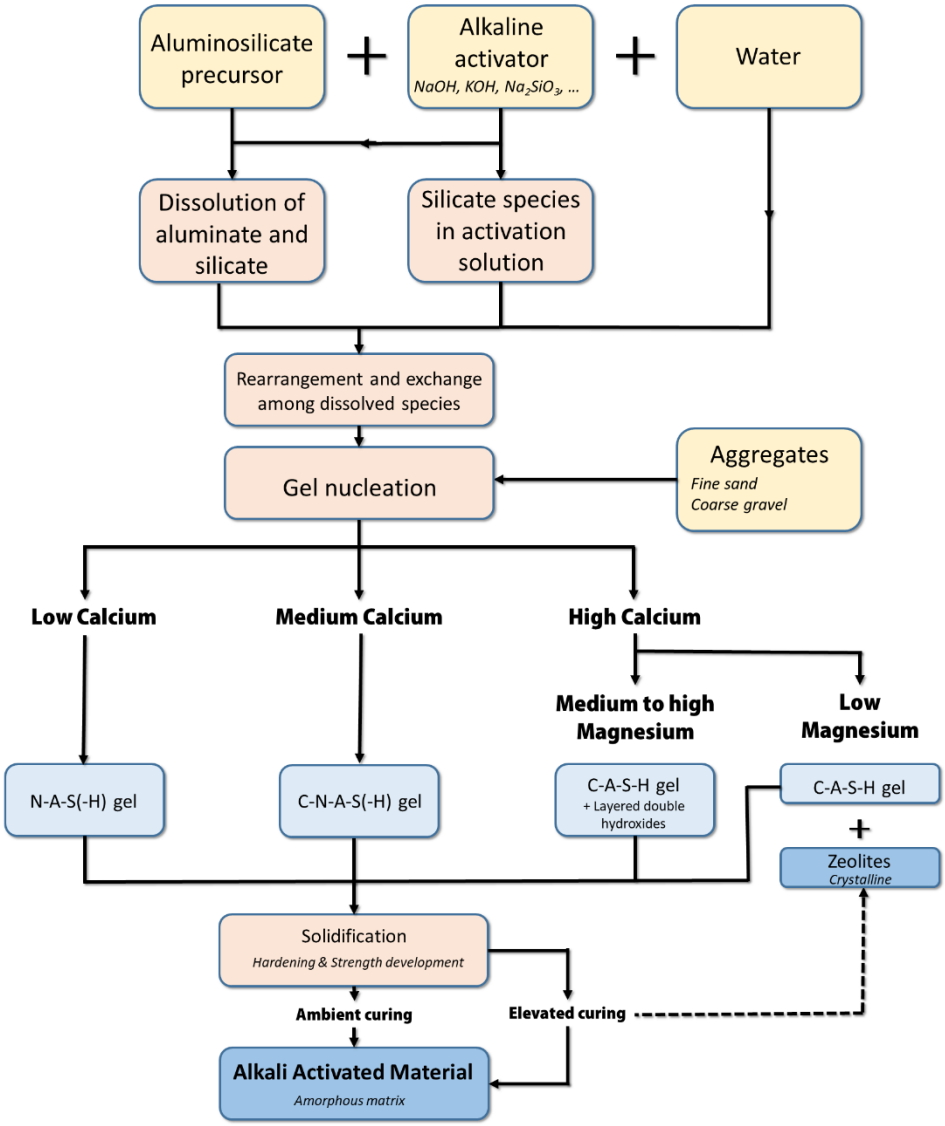

Figure 3: The alkali-activation process of an aluminosilicate source[10,11].

Alkali-activation technology has been recognized as an attractive option for immobilization of toxic or radioactive materials[11–14]. The high pH of the materials from 12 to 13 insolubilizes many metals and radioelements such as ^{137}Cs and protects metals from corrosion effects[2,15,16]. The use of AAMs for the immobilization of radioactive waste (RAW) is especially promising because of the low setting temperature (10-100 °C) and the lack of $Ca(OH)_2$ formation[17]. Additionally, these binders have promising properties as high chemical and temperature resistance[1,18,19]. The change in compressive strength at high exposure temperatures is shown in figure 4. Moreover, AAMs have a lower water content than OPC based binders and they can be almost completely dehydrated by heating at 300-400°C with no significant effect on the compressive strength, thus giving the ability to reduce radiolytic hydrogen yield.

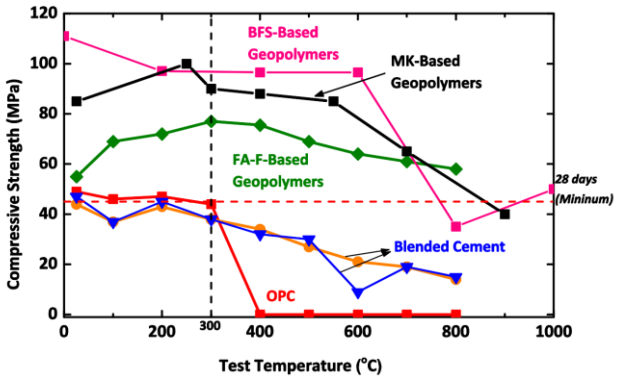

Figure 4: Change in compressive strength as a function of exposure temperatures for OPC based binders and geopolymer formulations (BFS: Blast furnace slag, FA-F[b]: class F fly ash, MK: Metakaolin)[11].

In 2013, the International Atomic Energy Agency (IAEA)[20] expressed its interest in four types of alternative cementitious materials for use in nuclear safety structures, including geopolymers, magnesium phosphate cements, calcium aluminate cements and calcium sulfoaluminate cements[21,22]. Also in 2013, the first paper describing the usage of a geopolymer for the encapsulation of Mg-Zr alloy was published by Rooses et al.[23]. They compared the radiolytic hydrogen yield of geopolymer samples to cement matrices and found a lower H_2 yield for geopolymer samples[23]. This is important since radiolytic dehydration can cause pressurization, spalling and micro-crack formation in the material matrix[24]. Moreover, hydrogen is highly flammable, thus giving a fire risk. Though promising, the use of geopolymer-type materials still requires precursor standardization, process optimization and validation for specific applications. The application as shielding materials and conditioning material for RAW will be discussed in section 2 and 3 respectively.

2. Alkali Activated Materials as a shielding material

Shielding materials are used to protect against damage caused by e.g. radiation. Besides the shielding capacity of the material, the durability, the economical and mechanical aspects of the material need to be considered[25]. Lead, for example, is a very good shielding material for ionizing radiation due to its high density and high atomic number. Therefore, lead shields only require a limited thickness to protect from ionizing radiation. The structural properties of lead (low strength exacerbated by its creep and fatigue behavior), however, do not allow its use as a structural material. Moreover, it is also sensitive to high temperatures[25]. Therefore, concrete-based shielding structure are mostly used in nuclear facilities. Concrete is regarded as an inexpensive material of which the shielding capacity can be adapted by adding different cements and aggregates. Aggregates, rich in iron or barium are most commonly used to create high density concretes (HDC) with high shielding capacities. The aggregates added to the matrices are expensive[9]. Fe-rich AAMs offer an interesting alternative to HDC, from an economical point of view, since the slags necessary to produce AAMs are about 10 times cheaper than the minerals used in HDC[9].

2.1. Shielding performance of AAMs

Currently, HDCs are used for shielding against ionizing radiation. As metallurgical slags also contain a large variety of elements with a high atomic number, the slags are potential raw materials for shielding. When using Fe-rich aluminosilicate precursors for AAM production, the iron can participate in the silicate network[8,26–28]. Fe^{3+} is situated in tetrahedral coordination, while Fe^{2+} is situated in an octahedral state[29]. Using Fe-rich precursors, a material with good shielding properties can be generated without the necessity

[b] Class F fly ash stands for a fly ash with a lime (CaO) content below 10% and consists mainly of alumina and silica.

to add expensive aggregates. The shielding capacity of materials is expressed as the linear attenuation coefficient (μ). Kaplan[25] defines this parameter as "the probability of an atomic particle or photon (X-ray or gamma-ray) interacting in a particular way with a given material per unit path length". μ depends on the type and energy of the incident radiation, the density and the composition of the interacting material[25]. μ is proportional to the number of atoms per unit of volume (N) and the cross section of the component (σ), expressed as $\mu = \sigma \cdot N$. Since μ is dependent on the density, the mass attenuation coefficient is often used which is the normalization of the linear attenuation coefficient per unit of density (μ/ρ). The higher the linear attenuation coefficient, the higher the shielding capacity of a material.

Croymans-Plaghki[9] compared the attenuation coefficient of fayalite slag based AAMs to different types of HDC. It was found that the fayalite based AAMs attenuated up to 28% better than ordinary, hematite-serpentine, ilmenite-limonite and basalt-magnetite concrete. At an energy of 1500 keV the linear attenuation coefficient of ordinary HDCs varied from 0.120 to 0.256 cm^{-1} (Figure 5). For the tested AAM, at 1500 keV a value of μ = 0.157 cm^{-1} was obtained, due to the higher effective atomic number (Z_{eff}) of this material compared to the ordinary HDCs. Only steel scrap and steel-magnetite concrete have a higher Z_{eff} and thus have a better shielding capacity. The linear attenuation of basalt-magnetite concretes was comparable to the linear attenuation of fayalite slag based AAMs. Mohammed et al.[30] compared the linear attenuation coefficients of an ordinary concrete and a fly ash based AAM and found a slightly smaller coefficient for the AAM samples, probably due to the lower specific gravity of the fly ash binder compared to the OPC binder. At 75 wt.% barite addition to the recipes, the AAM samples had a μ = 0.396 cm^{-1} at 663 keV and μ = 0.316 cm^{-1} at 1250 keV. For the OPC samples with 50 wt.% of barite, these values were respectively μ = 0.459 cm^{-1} and μ = 0.371 cm^{-1}. Fly-ash based AAMs were also investigated by Shalbi et al.[31] for application in radiation protection shield for X-ray attenuation. It was found that about 5 cm of fly ash based AAM with 15 wt.% $BaSO_4$ has the same attenuation ability of 1 mm of lead. Also activating a slag using $Ba(OH)_2$ could improve the shielding performance of an AAM[32].

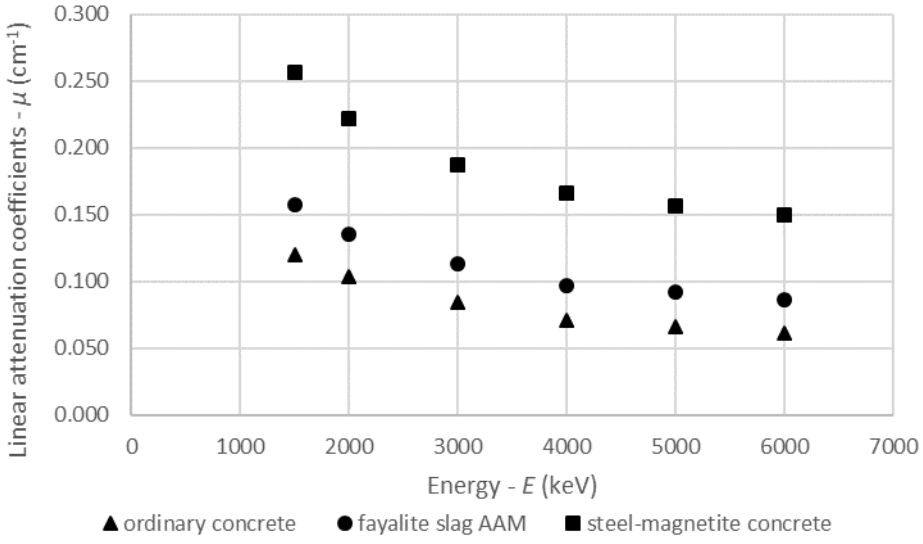

Figure 5: Linear attenuation coefficients of ordinary concrete, fayalite slag based AAM and steel-magnetite concrete as determined by EGSnrc based on research of Croymans-Plaghki[9].

The shielding performance of AAMs for neutrons can be improved when substituting boron for aluminum in the aluminum silicate network of the AAM. Williams et al.[33] named it, alkali activated boro(alumino)silicate inorganic polymers. They used borax ($Na_2B_4O_7$) as a boron containing feedstock.

Boron-10 is often used to capture thermal neutrons as it has a high absorption cross-section and a high natural abundancy. The macroscopic cross sections of the AAMs for thermal neutrons were comparable to these of borated polyethylene (PE) and superior to that of water. The advantage of the boro-AAMs compared to borated PE and water is the possible higher working temperature. Furthermore, boro-AAMs have the advantage not to become significantly radioactive due to neutron activation, reducing the need for additional shielding for gamma radiation, particularly if potassium is substituted for sodium[33]. When potassium is present, ^{40}K can be formed which has a very long half-life of 1.25×10^9 year. The shielding performance of lunar regolith[c] based AAMs was also investigated by Montes et al.[34] using shielding simulations. They showed that it is possible to create an AAM from lunar regolith with properties that would enable the construction of structures on the moon allowing for adequate radiation shielding inside the lunar living quarters.

Slag based AAMs are thus an interesting alternative to HDCs as shielding material since similar shielding capacities with respect to commercially available HDCs can be obtained with AAMs only using cheap materials as slags.

2.2. Effects on AAMs in a gamma irradiation field

Material properties can be altered due to irradiation. Damage might result from the breaking of chemical bonds or from the embrittlement of the material[35]. Due to irradiation, energy is deposited in the material causing heating, and moisture transport. Therefore, these effects should be considered when studying irradiation effects[36]. Radiolytic[d] dehydration is one of the important effects causing the formation of microcracks in cementitious materials[37]. Within 10^{-7} to 10^{-6} s after the start of gamma ray exposure, water decomposition results in the formation of eight primary species: H_2, H_2O_2, OH^-, H_3O^+, e_{aq}^-, $H^\bullet$, $OH^\bullet$ and $HO_2^\bullet$ [38] (Figure 6).

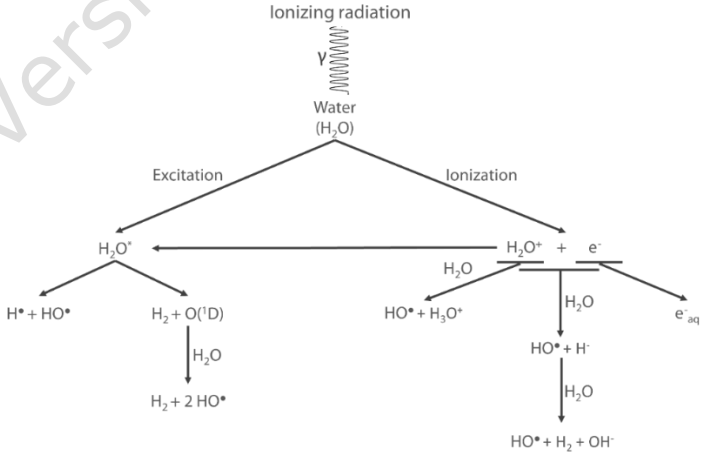

Figure 6: Radiolysis of water with the formation of ions, excited molecules, electrons and radicals – based on Le Caër[39]. In a first stage, ionized water molecules, excited water molecules and sub-excitations electrons are formed. Next, numerous processes occur as dissociative relaxation, ion-molecule reaction, autoionization of excited stated, thermalization of sub-excitation electron, etc. The species react in tracks and diffuse in the solution[39].

[c] Lunar regolith is the powder material which can be found on the surface of the moon.

[d] Radiolysis is the physicochemical results of ionization along the path of a gamma photon.

H_2 is the major stable product of water radiolysis. In a free volume at a pH = 13, the H_2 yield is 4.3 x 10^{-8} mol. J^{-1} for water[40]. However, the evolution of the primary species in time is highly dependent on the pH in alkaline environment (Figure 7). The primary G(H_2) can vary from 4.5 x 10^{-8} mol. J^{-1} to 4.0 x 10^{-8} mol. J^{-1} between pH 12.45 and 14[38].

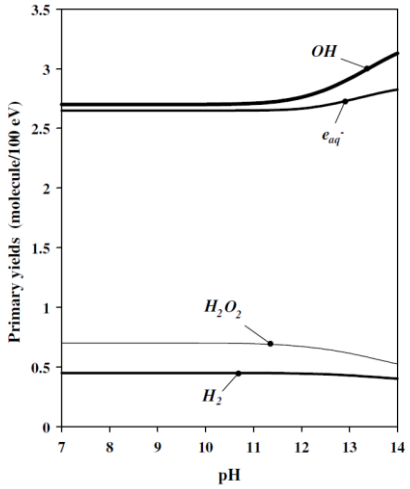

Figure 7: pH dependency of the yield of primary species resulting from water radiolysis at 25°C[38].

In cement, the hydrated calcium silicate hydrate (C-S-H) is the main strength-building phase of which water is a key-component. Radiolysis of the water leads to drying and therefore shrinking of the cement with the formation of micro cracks and thereby increase in the average pore diameter[41]. Dehydration thus can have a serious impact on the cement structure. For AAMs, no damage is reported when dehydration occurs[42]. AAMs are however microporous materials[43], meaning that water can be entrapped in the pores and can be the target of irradiation. In 2013, for the first time, metakaolin[e] based Na-geopolymer samples were exposed to γ radiation by Rooses et al.[23] to evaluate the radiolytic hydrogen yield. The hydrogen production in one-month-old-ambient-dried samples was evaluated for a dose rate of 600 Gy. h^{-1} up to 50 kGy. The apparent hydrogen production G(H_2) was 6.1 x 10^{-9} mol. J^{-1}. Later research of Lambertin et al.[44] using non-dehydrated samples (32.5 - 35.9 wt.% H_2O) however indicated a slightly higher apparent yield in the range of (0.9 – 1.1) x 10^{-8} mol. J^{-1} depending on the initial water content and the microstructure of the samples. Chupin et al.[45] and Cantarel et al.[46] found a value of respectively 1.4 x 10^{-8} mol. J^{-1} and 1.2 x 10^{-8} mol. J^{-1} for Na-metakaolin based geopolymers. This apparent yield is however still lower than the G(H_2) of 8.3 x 10^{-8} mol. J^{-1} found for OPC-matrices with a 28.6 wt.% H_2O content as reported by Bykov et al.[47]. An overview of the apparent hydrogen yield for different AAM recipes is given in table 1. It seems that the apparent yield for cement compounds is about twice this of free water. This is due to saturated salt solution present in in de cement. Salts as CaOH can participate in the radiation-chemical transformations interacting with H_2O_2 resulting in higher hydrogen gas production. For fly ash based geopolymers Leay et al.[48], even found a H_2 yield of (2.1 x 10^{-9}) mol. J^{-1}.

[e] Metakaolin is the dehydroxylated product of the mineral kaolin by heating to a temperature between 450 and 800°C.

Table 1: Overview of the apparent yield of radiolytic hydrogen gas normalized to the water content of different AAMs found in literature. The values are compared with this for free water and an OPC cement. *For free water, the apparent yield is equal to its real yield.

		Dose Rate (Gy. h^{-1})	**Dose (kGy)**	**Apparent $G(H_2)$ normalized to water content (x 10^{-8} mol. J^{-1})**
Bjergbakke et al.[49]	Free water (pH = 13)	/	/	4.3*
Rooses et al.[23]	Al_2O_3 3.6SiO_2 Na_2O 11H_2O	600	50	3.6
Rooses et al.[23]	Al_2O_3 3.6SiO_2 Na_2O 11H_2O (powder)	600	50	4.4
Lambertin et al.[44]	Al_2O_3 3.6SiO_2 Na_2O 11H_2O	600	750	2.8
Lambertin et al.[44]	Al_2O_3 3.6SiO_2 Na_2O 12H_2O	600	750	3.0
Lambertin et al.[44]	Al_2O_3 3.6SiO_2 Na_2O 13H_2O	600	750	3.1
Chupin et al.[45]	Al_2O_3 4SiO_2 Na_2O 12H_2O	5000	600	4.2
Cantarel et al.[46]	Al_2O_3 3.8SiO_2 Na_2O 13H_2O	2200	0-10	3.5
Cantarel et al.[46]	Al_2O_3 3.8SiO_2 Na_2O 13H_2O (powder)	2200	0-10	5.8
Leay et al.[48]	Fly ash AAM - 1.3Al_2O_3 10SiO_2 Na_2O 11H_2O	24000	400-700	0.9
Leay et al.[48]	Fly ash AAM - 1.0Al_2O_3 8SiO_2 Na_2O 11H_2O	24000	400-700	0.7
Leay et al.[48]	Fly ash AAM - 0.8Al_2O_3 7SiO_2 Na_2O 11H_2O	24000	400-700	0.6
Bykov et al.[47]	OPC cement (water/cement = 0.4)	5700	855	29.0

Chupin et al.[15] investigated the processes controlling the H_2 production and the relationship to the geopolymer composition when irradiated. A metakaolin geopolymer was activated with NaOH, KOH and/or $CsOH.H_2O$. The samples were cured at various relative humidity using the saturated salt method. The samples were sealed and irradiated using a ^{60}Co source at 500 Gy. h^{-1} until a total absorbed dose between 114 and 517 kGy. From this study, Chupin et al.[15] concludes that water in geopolymers can be decomposed under irradiation whether it is bulk water or not. All the different forms of water in a geopolymer can be decomposed. The H_2 yield is proportional to the initial water content of the sample. However, this statement is not valid for saturated samples since the diffusion coefficient of H_2 in a saturated geopolymer is 100 to 1000 times lower than in an unsaturated sample[46,50]. When diffusion is very low, an equilibrium state can be established in the sample so that all new hydrogen produced will recombine (Figure 8). This is also the case for encapsulated waste. An equilibrium is established since the new production of H_2 is compensated by the decomposition of H_2 by $O^{\bullet -}$. This is not possible in an open system, since the concentration of H_2 related to O_2 will never be high enough to cause decomposition of H_2. The equilibrium state limits the hydrostatic pressure build up in the sample and limits the risk of cracking. Moreover, additional sources of H_2 as e.g. steel corrosion will only have a limited effect. Radiolytic yield thus also depends on the scale of the waste package since less H_2 will reach the surface of a large package and so equilibrium will be reached faster. Also, the maximum concentration of hydrogen is proportional to the dose rate reached in the sample[46].

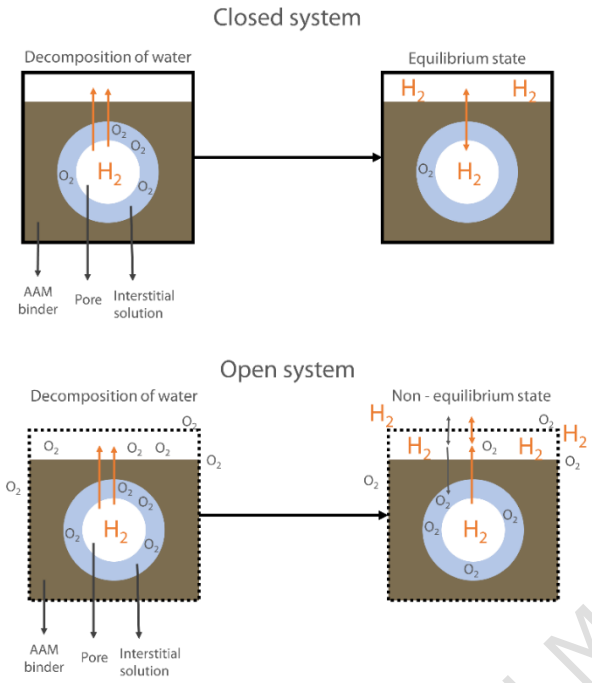

Figure 8: Schematic overview of the (non) equilibrium state of H_2 in a closed and open system – based on a study of Chupin[45].

In general, the water radiolysis increases with decreasing pore sizes and increases with increasing specific surface area[48]. Smaller pores lead to a larger specific surface and so to a larger solid-to-liquid interface area. Since more excitations take place at the pore wall interfaces, also, more H_2 will be produced when a larger interface area is present[51]. This is because of the Compton electrons diffusion at the solid-liquid interface which induces a higher energy to be deposited in the pore water due to the different electronic density of the solid and the liquid. Larger interface area leads to more excitons and thus more energy which is transferred to the adsorbed water at the pore surface and thus leads to a higher hydrogen gas yield[46,52]. This causes the radiolysis of water to be more efficient in entrapped water than in bulk water[52]. In AAMs, the adsorbed water on the pore walls receives energy from direct gamma ray interaction and from solid-to-liquid excitons transfers. The water at the center of the pores is similar to free water and only receives energy from direct ionizations by gamma rays[15]. The recombination probability of H• radicals (eq. 1) and hydrated excitons (eq. 2) formed under gamma irradiation is larger in small pores, leading to a higher H_2 yield[51]. This effect is however only dominant for pores smaller than 25 nm[51]. The effect of radiolysis is in literature often reported as an increased water loss compared to non-irradiated samples and thus an accelerated dehydration[53,54]. Introducing elements with a higher atomic number into the AAM causes the mean atomic number to increase and therefore also the electronic density of the solid matrix. This leads to a higher energy deposition, a better shielding, and thus a higher H_2 yield[15]. Moreover, by increasing the size of the cation ($Na^+ < K^+ < Cs^+$), smaller alumino-silicates oligomers are formed, and a finer and more uniform pore network is created thus also increasing the H_2 yield[15]. Mainly the porosity (pore size distribution and specific surface area) and the mean atomic number of the solid matrix of the geopolymer thus affect the hydrogen production. This effect was earlier observed by Le Caër et al.[51] in controlled-pore glasses.

$$H^{\cdot} + H^{\cdot} \rightarrow H_2 \qquad \text{(eq. 1)}$$

$$e^-_{aq} + e^-_{aq} \rightarrow H_2 + 2OH^- \qquad \text{(eq. 2)}$$

H_2 formation as a result of homolytic breaking of the OH bond in silanol groups (-SiOH), as proposed by Le Caër et al.[51], is negligible for AAMs since silanol groups are expected to be present as silanolate ($-SiO^-$) groups because of the high pH of AAMs. A more important effect for AAMs is the change in H_2 yield due to dissolved ionic species in the pore water as calcium and iron[38,48,55]. Cantarel et al.[46] found that the H_2 yield decreases when the concentration of the ionic species in the pore solution increases, for example due to drying of the AAM. However, large differences in concentrations only lead to a small effect on the yield. An overview of the different parameters affecting the hydrogen yield of an AAM sample is given in table 2.

Table 2: Summary of the properties affecting the apparent radiolytic hydrogen yield.

	Properties affecting the hydrogen yield
1	The pH of the pore water;
2	The initial water content;
3	The possibility to reach an equilibrium state;
4	The dose rate in the sample;
5	The pore size distribution and specific surface of the sample;
6	The mean atomic number of the solid matrix;
7	The concentration of ionic species in the pore solution.

Lambertin et al.[44] irradiated metakaolin Na-geopolymers at a dose rate of 600 Gy. h^{-1} until 750 kGy under an argon atmosphere at ambient conditions. An increase of the compressive strength with 10% was observed, probably as a result of a densification of the structure under gamma irradiation. A broader range of pores sizes was observed after irradiation with the appearance of two peaks in the pore size distribution (PSD) (Figure 9) after irradiation compared to the non-irradiated samples. An explanation for this phenomenon could be the reorganization of the thin pore walls. The total pore volume however does not change with irradiation[44]. A change in PSD was also observed by other researchers. Deng et al. [56] irradiated class F AAMs using a ^{60}Co source (700 Gy. h^{-1}) to a cumulative dose of 100 kGy. A decrease of the pore population from 0.2-7 µm was observed in favor of the smaller and larger pores in the regions 40-200 nm and 7-40 µm[56]. Mubasher et al.[54] found a decrease in porosity of metakaolin based geopolymer due to irradiation at 21 kGy. h^{-1} using a ^{60}Co source. Mast et al.[53] irradiated plasma slag based AAMs 1 hour after casting using a ^{137}Cs source with a dose rate of 152 Gy. h^{-1} and found a shift in the PSD towards the smaller pores (< 10 nm) compared to non-irradiated samples.

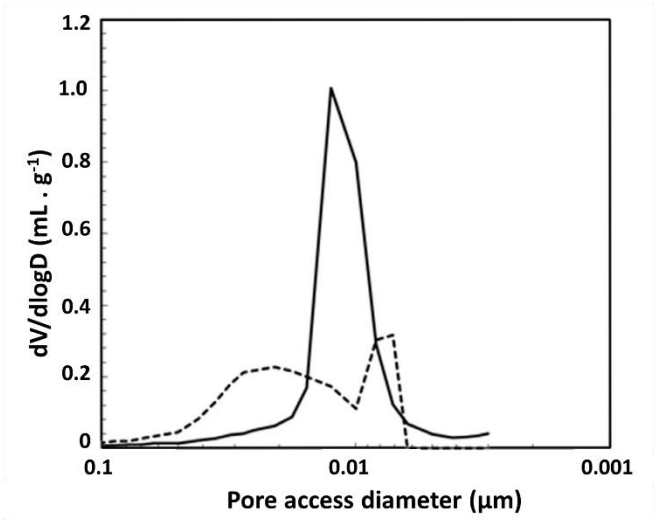

Figure 9: The pore access diameter distribution of an irradiated Na-geopolymer (dotted line) and a non-irradiated Na-geopolymer (solid line) measured with mercury intrusion porosimetry[44]. The pore access diameter is the equivalent diameter for the pore entrance which corresponds to the interconnections between pores, rather than the internal pore diameter.

The changes in compressive strength, microstructure and pore size distribution of AAM are attributed to the radiolysis of water, the reorganization of pore walls and a decrease in the average T-O (T = Si or Al in tetrahedral site) bonding angle[44]. The relaxation of bridging bond Si-O-Si angles is also observed in silica glasses under gamma irradiation[57,58]. Due to relaxation, a part of the energy stored in the structure is released causing a densification of the structure. Given that the silica structure is in a non-thermal equilibrium state and has an excess of energy stored in its bridging bonds, ionizing radiation produces electron-hole pairs enabling bonds to rearrange for structural relaxation. No crystalline phases will however be formed as a result of gamma ray interaction[56,59].

An increased compressive strength as reported by Lambertin et al.[44] was also found by Mast et al.[53] who irradiated plasma slag based AAMs using different dose rates (1.6 Gy. h^{-1}, 7.1 Gy. h^{-1}, 152 Gy. h^{-1} and 2 kGy. h^{-1}) until different absorbed doses with a maximum of 624 kGy. An increase was found for all the AAM samples when irradiated to an absorbed dose higher than 5 kGy. For the samples irradiated 24 h after casting at 2 kGy. h^{-1} an increased strength from 16% to 23% depending on de absorbed dose was reported. A similar experiment was executed by Craeye et al.[60] to evaluate the effect of gamma irradiation on self-compacting mortar. They found a decrease in compressive strength for all the samples, with a maximum decrease of 16.3%. This indicates that AAMs, from a mechanical point of view, are better resistant to gamma irradiation when irradiated at the early age. The increase in strength can be related to the growth of carbonates e.g. $CaCO_3$ or Na_2CO_3 in the microcracks and pores[36,61]. Or, can be related to the different oxidation states of iron, when using iron rich slags for alkali activation. It is known that in alkaline conditions under gamma irradiation, changes to the iron oxidation state occur [62,63].

2.3. Effects on AAMs in an electron irradiation field

Chupin et al.[15] performed electron irradiations with (i) a constant beam between 0.4 and 20 MGy. h^{-1} and a total dose between 0.5 and 301 MGy and with (ii) a pulsed beam with a dose of 30 Gy per pulse at 10 Hz frequency up to a total dose between 15 and 45 kGy. No crystallization effects and no changes in pore size distributions were observed. No stable radicals were created under electron irradiation. Three types of radicals were observed in the pulsed beam set up: $H^{\bullet}$ radicals, $Si\text{-}O^{\bullet}/H^{+}$ and $Al\text{-}O^{\bullet}/H^{+}$ defects and trapped electrons in the AAM network. The species are however very reactive and recombine very quickly.

2.4. Effects on AAMs in an alpha particle irradiation field

Chupin et al.[15] performed heavy ion irradiation to simulate the effect of incident alpha particles on the material. In their study thin pieces of metakaolin based geopolymer of 0.15 g were kept under argon and irradiated with a 95 MeV. amu^{-1} ^{36}Ar ion beam with a flux of 3.48 x 10^{8} ions. cm^{-2}. s^{-1} corresponding to a dose rate of 0.5 MGy. h^{-1}. Crystallization was observed in the geopolymer structure due to the nuclear elastic shock. The movement of atoms promotes the reorganization of the network in a crystalline structure.

The crystal phase formed (about +3% after 1 MGy) under heavy ion irradiation however depends on the cation present in the network. The activation energy for crystallization is dependent on the cation part of the crystalline structure: e.g. nepheline[f] for Na (250 kJ. mol^{-1}) and leucite[g] for K (1450 kJ. mol^{-1}). The crystalline phases are however not identical to the ones formed by thermal treatment. Nepheline structures can be observed as needle formation in the irradiated geopolymer samples[45].

A small change in the PSD was detected, probably due to the crystallization of the structure. The change in the porosity is however also highly dependent on the cation in the AAM structure since the crystalline phase formed plays a major role in the intergranular porosity. Irradiation with ^{36}Ar ions causes the pore volume to decrease with the formation of new peaks in the PSD related to the crystalline phases. For Na-geopolymers an extra peak appears at 17.5 nm related to the formation of nepheline. For the K-geopolymers peaks appear at 11.0 and 17.5 nm related to kaliophilite and nepheline. For Cs based geopolymers a change in the 3 to 4 nm region was observed related to the formation of pollucite. In all cases, the total pore volume decreases which could indicate the closure of some pores[15].

The H_2 yield obtained for a Na-geopolymer was 1.8 x 10^{-8} mol. J^{-1}, which is about four times higher than when irradiated with gamma rays. This is close to the $(G(H_2)_{alpha}$ particles/$G(H_2)_{\gamma\text{-rays}})$-ratio of 3.4 for free water at high pH, which indicates that the specific surface and porosity do not influence the H_2 yield for high LET[h] irradiation. This is since high LET radiation lead to a dense ionization track and thus a high probability of recombination before the excitons reach the pore surface. For high LET radiation, a reduced number of exciton transfers are therefore thought to take place compared to gamma irradiation. The radiolytic yield increased linearly with the water mass fraction in the original sample[15].

[f] $Na_3K(Si_{0.56}Al_{0.44})_8O_{16}$
[g] $KAlSi_2O_6$
[h] Linear Energy Transfer: The amount of energy which is deposited by a ionizing particle per unit of distance.

2.5. Effects on AAMs in a neutron irradiation field

AAMs form interesting materials for neutron shielding as they contain a lot of hydroxyl ions of which the protons can slow down the neutrons by elastic collisions and capture the thermal neutrons[64]. An AAM with an excellent neutron absorption capacity was designed by Takeda et al.[64]. They produced fly ash based AAMs of 10 mm thick and irradiated the samples for 15 min using neutrons with an intensity of 1.9×10^4 n. cm^{-2}. s^{-1}. μA^{-1}. The samples were only irradiated from one side and both sides were provided with a gold filament. After irradiation the difference in radiant intensities between the two gamma beams from the gold filaments was used to evaluate the neutron transmission of the AAMs. The results were compared with fresh OPC samples and 30 years old OPC samples. Fresh cement had the highest absorption ratio (0.282) for neutrons due to the high amount of water molecules in the paste. In contrast, the aged concrete had the lowest absorption coefficient (0.054) as a result of dehydration. Both AAM samples produced by the conventional method (0.198) or by warm pressing method (0.241) had a better absorption ratio than the aged OPC concrete. Warm pressed AAMs had a slightly lower absorption ratio for neutrons in comparison to the fresh OPC samples. It is however shown that AAMs lose less water over time compared to OPC samples as water can remain for a long time in the amorphous, zeolite-like structure of the AAMs. It is therefore expected that on a longer time scale the warm pressed AAMs perform better than the fresh OPC samples.

AAMs with high shielding capacities for neutrons can be designed by substituting boron for aluminum in the AAM description[33]. The boro(alumino)silicate inorganic polymers have a high macroscopic cross section for thermal neutrons due to the high absorption cross section of thermal neutrons for ^{10}B and the high natural abundance of ^{10}B.

When designing AAMs for neutron shielding, neutron activation of elements present in the material have to be taken into account. Elements which produce radioactivity-hazardous nuclides in a neutron irradiation field have to be avoided (table 3). Iron, cobalt, nickel, carbon, lithium, europium, calcium and cesium are known to form long-lived radionuclides due to neutron activation[65]. The induced radioactivity is determined by the main chemical elements, but also impurities (0.01-1 wt.%) and trace elements (<0.01 wt.%) can have a large contribution to the final activity of the material[66].

The contribution of the different radionuclides to the total activity of the material will be different on one- or another-time interval due to the different half-lives of the radionuclides. In the first 25 years after the neutron activation ^3H, ^{154}Eu, ^{60}Co, ^{55}Fe and ^{134}Cs play a major role in the determination of the total activity of the activated material. From 25 to 100 years mainly ^3H, ^{152}Eu and ^{63}Ni are the contributors to the total activity. On the long term (> 100 years) the long-lived radionuclides as ^{41}Ca, ^{233}U, ^{59}Ni, ^{239}Pu, ^{94}Nb and ^{63}Ni are hazardous radionuclides. In concrete mainly the presence of stable calcium in a large quantities is problematic[66].

Table 3: Characteristics of the most important radionuclides present in materials subjected to neutron irradiation ordered according to descending half-life value (The darker the color, the more important the radionuclide in terms of half-life or in terms of specific activity) – based on Bylkin et al.[65].

Parent	Formation reaction	Hazardous radionuclide	Decay	Half-live (year)	Specific activity (Bq. g^{-1})
^{35}Cl	^{35}Cl (n, γ) ^{36}Cl	^{36}Cl	(β^-, 98.1%) (β^+, ε, 1.9%)	3.0 x 10^5	1.2 x 10^9
^{232}Th	^{232}Th (n, γ) ^{233}U	^{233}U	(α, 100%)	1.6 x 10^5	3.6 x 10^8
^{40}Ca	^{40}Ca (n, γ) ^{41}Ca	^{41}Ca	(ε, 100%)	1.0 x 10^5	3.2 x 10^9
^{58}Ni	^{58}Ni (n, γ) ^{59}Ni	^{59}Ni	(β^+, ε, 100%)	7.6 x 10^4	3.0 x 10^9
^{238}U	^{239}U (n, γ) ^{239}Pu	^{239}Pu	(α, 100%)	2.4 x 10^4	2.3 x 10^9
^{93}Nb	^{93}Nb (n, γ) ^{94}Nb	^{94}Nb	(β^-, 100%)	2.0 x 10^4	7.0 x 10^9
^{13}C	^{3}C (n, γ) ^{14}C	^{14}C	(β^-, 100%)	5.7 x 10 ^{3}	1.7 x 10^{11}
^{62}Ni	^{62}Ni (n, γ) ^{63}Ni	^{63}Ni	(β^-, 100%)	9.9 x 10^1	2.1 x 10^{12}
^{151}Eu	^{151}Eu (n, γ) ^{152}Eu	^{152}Eu	(β^+, ε, 72.1%) (β^-, 27.9%)	1.4 x 10^1	6.4 x 10^{12}
^{6}Li	^{6}Li (n, p) ^{3}H	^{3}H	(β^-, 100%)	1.2 x 10^1	3.6 x 10^{14}
^{132}Ba	^{132}Ba (n, γ) ^{133}Ba	^{133}Ba	(ε, 100%)	1.1 x 10^1	9.4 x 10^{12}
^{153}Eu	^{153}Eu (n, γ) ^{154}Eu	^{154}Eu	(β^-, 99.982%) (ε, 0.018%)	8.6	1.0 x 10^{13}
^{59}Co	^{59}Co (n, γ) ^{60}Co	^{60}Co	(β^-, 100%)	5.3	4.2 x 10^{13}
^{54}Fe	^{54}Fe (n, γ) ^{55}Fe	^{55}Fe	(ε, 100%)	2.8	8.8 x 10^{13}
^{133}Cs	^{133}Cs (n, γ) ^{134}Cs	^{134}Cs	(β^-, 99.9997%) (ε, 0.0003%)	2.1	4.8 x 10^{13}

In concrete, used as bioshield in a nuclear reactor, the total activity on the 100-year time scale is dominated by tritium (Figure 10 - i), while on the long-term time scale the activity is dominated by ^{41}Ca (Figure 10 - ii). The gamma activity is mainly attributed to ^{152}Eu. For most of the AAM definitions, the amount of calcium in the aluminosilicate precursors is significantly lower than for OPC. In metakaolin for example, the CaO-content is limited to < 0.5 wt.%. The formation of the long lived ^{41}Ca as a result of neutron activation will therefore be limited in geopolymers. A problem with using aluminosilicate precursors can be the slightly higher iron, barium and potassium content. The latter could form ^{40}K with a half-life of 1.2 x 10^9 year. Also traces of ZrO_2 are undesirable since they will lead to the production of ^{93}Zr with a half-life of 1.6 x 10^6 year.

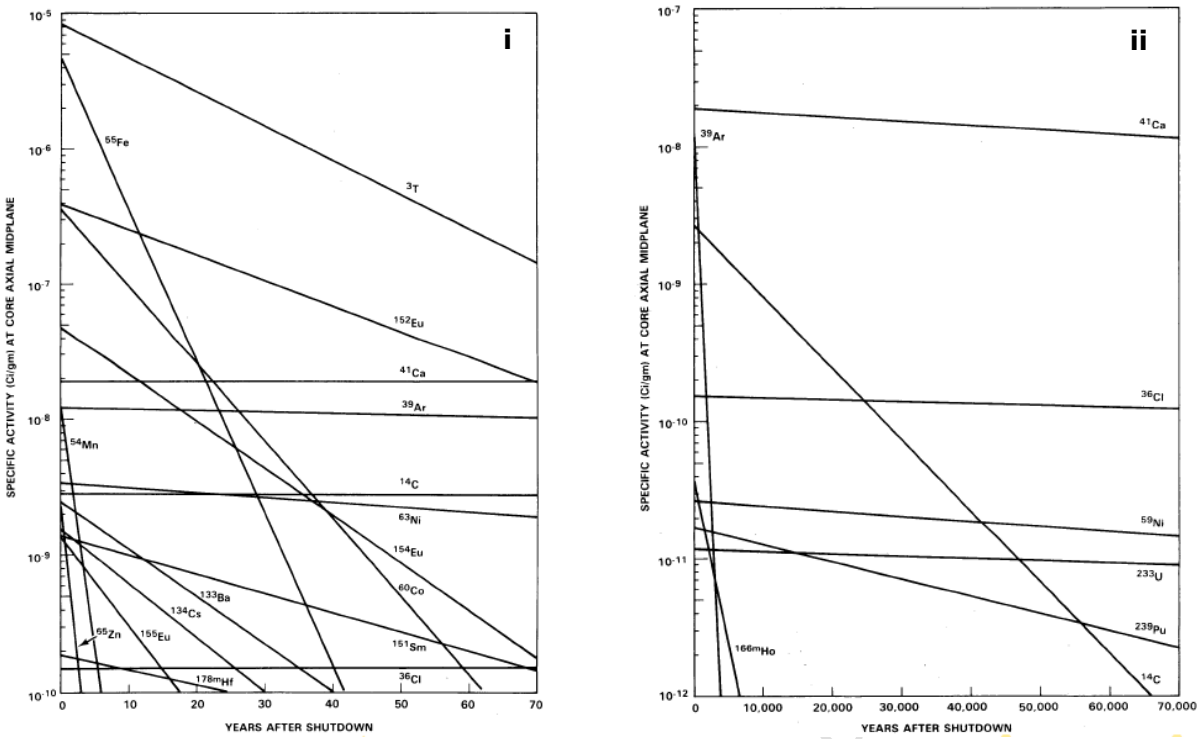

Figure 10: The specific activity of the radionuclides present in a concrete pressurised water reactor bioshield at 10 cm depth, x years after the shutdown indicated (i) on the short term & (ii) on the long term[67].

3. Alkali Activated Materials as conditioning material

Low-cost, low-temperature processes as bituminization and cementation are currently used worldwide to immobilize low-level radioactive waste (LLW) and intermediate-level radioactive waste (ILW). In this section, the potential of AAMs to replace the standard OPC-based mixtures to contain LLW and ILW is discussed.

AAMs have certainly several properties, making them interesting candidates for the conditioning of certain radioactive waste streams.

- The absence of portlandite ($Ca(OH)_2$) in AAMs is expected to be beneficial for the immobilization, since portlandite has only a weak immobilization potential.
- The water content of AAMs can be significantly reduced by heating the samples and thus reducing the radiolytic hydrogen yield and avoiding freeze-thaw problems.
- The high alkalinity of AAMs can cause formation of insoluble hydroxides for many actinides and fission products, providing a good immobilization[14]. The high alkalinity however can also cause the corrosion of reactive metals leading to hydrogen formation. In this case, low alkaline AAMs need to be used such as AAMs activated with Na_2CO_3 or Na_2SO_4[68].
- AAMs have an excellent fire resistance[69,70].

Also, several immobilization mechanisms have been reported in literature.

- AAMs can immobilize monovalent cations (e.g. Cs^+) as a charge-balancing ion in their structure and replace Na^+ or K^+ [71,72]. The replacement of Na^+ by Sr^{2+} is also reported[73].
- Monovalent or bivalent cations (e.g. Sr^{2+}) can be incorporated in C-S-H phase replacing Ca^{2+} [74,75].
- Ions can be incorporated in (N(-C)-A-S(-H) amorphous aluminosilicate structure of the AAMs[16,17,76–79].
- Radioactive elements can be incorporated in crystalline phases[79–82].
- Due to the high alkalinity of AAMs, the formation of precipitates as hydroxides or carbonates is promoted[16,76–78,83].
- Radionuclides can be adsorbed on introduced or self-generated zeolite[i] structures in AAMs[73,75,84,85].
- Chemisorption and electrostatic interactions with the AAM binder leads to a low leachability of radionuclides[83].
- Low radionuclide leachability of AAMs is related to their low porosity and low critical pore diameter[81,86,87].

Since there is a wide variety of RAW streams and moreover a wide variety in possible definitions of an AAM to immobilize a specific waste stream, the following part will discuss each kind of waste stream separately with the focus on the immobilization mechanisms of the chosen system.

[i] Zeolites are microporous aluminosilicate minerals commercially used as adsorbents.

The different kinds of radioactive waste streams which are discussed are:

Liquid wastes:

- Organic liquids
- Aqueous waste
    - Contaminated water with cesium and strontium
    - Sulphate rich aqueous waste

Solid wastes:

- Zeolites
- Aluminum containing waste
- Mg-alloys

3.1. Liquid wastes

Organic liquids

In previous studies, it was shown that liquid organic wastes have a significant effect on the properties of cementitious materials[88,89]. Moreover, organic liquids could easily be released during mixing or curing. Addition of organic liquids to the cement paste causes delayed setting and hardening and slows down the overall processes. The use of sorbents, as active coals ore clays, is necessary to avoid the organic liquid to leach out[88]. Even at low concentrations, organics can already affect the properties of hydrating cement[89]. Moreover, only 12 (v/v)% of oil can be incorporated directly into cement to still obtain a solid and dry waste form[90]. Additional emulsifiers can be used to increase the waste loading capacity. Greenhalgh incorporated up to 40 (v/v)% of waste by the use of emulsifiers.

Cantarel et al.[91] studied the possibility of incorporating liquid organic oil waste in a metakaolin based geopolymers. The process consists of the emulsification of oil in an alkali solution and next adding it to an aluminosilicate source, for example metakaolin to create a geopolymer. This procedure was patented by Lambertin et al.[92]. Cantarel et al.[91] succeeded to add up to 20 (v/v)% of oil waste into the geopolymer. It was found that the oil was present in the matrix as small droplet ranging from 10 to 50 μm which were homogeneously dispersed. The droplets are formed from the moment the oil is added to the alkaline solution, indicating a good emulsification by the activating solution. When mixing both solutions, the alkali from the activator reacts with the alkanoic acids from the oil, producing in situ surfactants which reduce the interfacial tension between water and the oil. No escape of oil was observed during and after setting. The setting time however tends to increase with increasing oil content, since OH^- is consumed by the acids in the oil thus slowing down the reaction. The resulting oil/geopolymer composites however had good mechanical properties of >22 MPa in compressive strength after 30 days. The higher the oil volume fraction, the lower the final strength of the samples. Also, an increase in the viscoelasticity and elasticity can be observed. Though, it is stated by Cantarel[93] that chemical and mechanical kinetics of the hardening process are not affected by the oil as long as no acids are present in the oil. There is no chemical interaction observed between the oil and the geopolymer. The structure of the geopolymer was not affected and was identical to that of a pure geopolymer. However, surfactant molecules have to be added to the recipe to obtain a homogeneous material. It is also reported that organic oil does not affect the geopolymer hardening rate, the kinetics and mechanisms of formation of the porous network[94]. Below 27 (v/v)%, a non-percolating network can be achieved according to Davy et al.[95].

Contaminated water (with cesium and strontium)

Nuclear fuel reprocessing activities produce liquid RAW commonly referred to as sodium-bearing waste with ^{90}Sr and ^{137}Cs as dominating radionuclides[96]. Li et al.[97] used contaminated water directly to create a paper sludge fly ash based alkali activated material with low Ca content. Paper sludge fly ash mixed with solid $Sr(NO_3)_2$ and $CsNO_3$ was activated with $Na_2O{\cdot}2SiO_2{\cdot}aq$. High immobilization ratios for Cs^+ and Sr^{2+} were reached. It is thought that the ions are incorporated into the AAM-gel or into faujasite (Figure 11) which is a member of the zeolite family. Both Cs^+ and Sr^{2+} can be entrapped in the sodalite cages of faujasite since the cages have an opening diameter of 0.74 nm which is larger than the ionic radii of Cs^+ and Sr^{2+} [97]. Faujasite is, however, only present in small amounts compared to the geopolymer AAM-gel. Cs^+ could, therefore, also be incorporated in the N-A-S-H gel, while Sr^{2+} could interchange with Ca^{2+} in the C-A-S-H gel. Due to the presence of Ca^{2+}, ion exchange of Na^+ for Ca^{2+} can occur in the N-A-S-H gel, what makes the phase unstable in time. Therefore, the immobilization of Cs^+ could decrease with the ion exchange of Na^+ with Ca^{2+}. Sodium- and nitrate-bearing liquid waste was successfully immobilized by Wang et al.[96] using metakaolin, class F fly ash and blast furnace slag. The nonradioactive ^{133}Cs and ^{88}Sr were introduced as nitrated and were dissolved in nitric acid. The solution was alkalized to a pH of 12-13 using NaOH and next mixed with the raw materials to prepare an alkali-activated-slag-fly ash-metakaolin hydroceramic. Most of the cations were incorporated in the crystalline zeolite structures and captured in the voids and channels. Analcime[j] was the major crystalline phase detected. The addition of the liquid waste was beneficial for the formation of the analcime zeolites due to the additional cations from the waste. Cations are necessary to form zeolites, but not enough cations were present in the raw materials. The formation of the analcime phase was thus promoted by adding the cation rich waste stream[96].

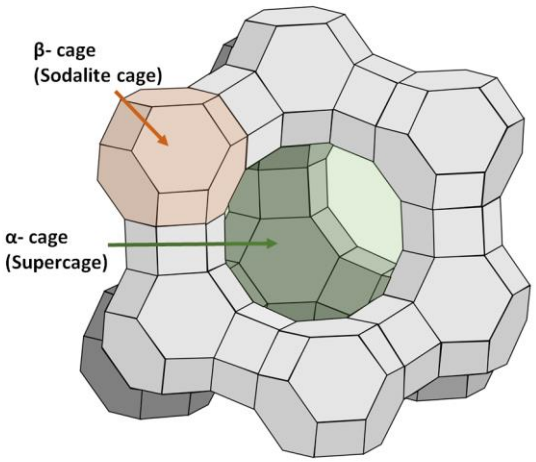

Figure 11: 3D structure of zeolite Y also called faujasite with sodalite cages.

Another way of immobilizing radioactive cesium which was already reported in 1981 by Gallagher et al.[98] is the firing of cesium oxide together with an alumina and silica source to generate pollucite ($CsAlSi_2O_6$). The role of cesium in the formation of the crystalline phases was studied by Chlique et al.[79]. They prepared samples using a mix of liquid CsOH and NaOH to activate metakaolin. The samples were then heated to 1100°C. It was found that 75 wt.% of the crystals were pollucite ($CsAlSi_2O_6$) and 25 wt.% feldspathoid ($CsAlSiO_4$). Arbel-Haddad et al.[99] however found that at low Si content [$SiO_2/Al_2O_3 < 2$], cesium bearing crystalline phases can also be formed at ambient temperature, eliminating the necessity for high

[j] Analcime consists of hydrated $NaAlSiO_6$ in cubic crystalline form.

temperature treatment[100]. Arbel-Haddad et al.[99] found that mainly cesium bearing zeolite A[k] and zeolite F[l] was formed in nitrate free samples. Nitrate cancrinite was the major phase for nitrate bearing samples[101]. Ofer-Rozovsky et al.[101] showed a lower Cs- and a lower Na-leaching of Nitrate cancrinite compared to zeolite A, indicating that the addition of $NaNO_3$ to the geopolymer could be beneficial for the immobilization of cesium[102]. Cs is located in the cancrinite cages. The cage has an almost perfect size to fit a cesium ion coordinated to the 12 surrounding oxygen atoms[103]. Smaller ions can be located on more than one position in the cage[103]. The cesium ions are well kept in the structure and cannot leach out since they cannot pass through the ring[103]. Sodium in the cancrinite structures was not easily exchanged with Cs^+ [104]. Nitrate cancrinite and nitrate sodalite are reported as being good minerals for cesium retention[105]. The Cs^+ is trapped in the cages and channels of the minerals. Moreover, Cs^+ has a higher ionic radius compared to Na^+ which therefore results in a hydration shell which is less bounded, whereby cesium ions may more easily dehydrate and bind to the aluminate groups of the zeolites or the geopolymer gel. There is however an enhanced selectivity for cesium ions provided by nitrate cancrinite and nitrate sodalite which is not well understood yet.

Ofer-Rozovsky et al.[101] studied the immobilization of Cs^+ by low-Si geopolymers with the presence of nitrate, an anion often present in low-level nuclear waste. The formation of nitrate-bearing feldspathoid, nitrate sodalite and nitrate cancrinite was observed as it was also the case for Cs-free geopolymers[106]. Ofer-Rozovsky et al.[101] could not identify the formation of zeolite F. This is related to the fact that the concentration of nitrates was high compared to cesium so that the nitrate ion appeared as a more important structure-directing agent compared to the cesium ion. Since the concentration of Cs^+ in low-level nuclear wastes is even lower than the one used by Ofer-Rozovsky et al.[101], it is expected that also in the conditioning of low-level waste, nitrate will appear as a structuring agent and thus no zeolite F is expected to be formed.

The effect of cesium on the geopolymer matrix itself was studied by Berger et al.[107], Vandevenne et al.[16] and Provis et al.[77]. It was found that the use of cesium used as an activator, added as CsOH, slows down the reaction of alkali-activation compared to Na or K, leading to a longer setting time but also less unreacted raw material. A lower compressive strength was found for cesium bearing AAMs probably related to the less bounded hydration sphere[107]. When Cs however is added as CsOH on top of the standard activation solution, the higher basicity of the activating solution leads to a faster dissolution and faster gelation process. This was however not the case when the cesium was introduced as a nitrate[16] or a sulphate[77]. In both cases a slight retardation of the reaction was observed by Provis et al.[77] while no significant effect of $CsNO_3$ was observed by Vandevenne et al.[16]. In the case of $Sr(NO_3)_2$ however, the reaction kinetics were severely affected. The dissolution of the precursor was reduced due to the consumption of hydroxides by strontium for the formation of $Sr(OH)_2$, leading to a disruption in the development of the pore network[77] and a lower compressive strength[16]. It is proposed that Sr^{2+} will behave in a similar way as Ca^{2+} during alkali-activation[77]. When added as insoluble $Sr(OH)_2$, the formation of anhydrous $Sr(OH)_2{\cdot}8H_2O$ will lead to the removal of water out of the reaction system thus retarding the dissolution process of the precursor but accelerating the gel formation[77]. Addition of $SrSO_4$ may lead to the liberation of SO_4^{2-} when converted to $SrCO_3$ by atmospheric carbonation and affecting the reaction kinetics[5].

[k] Zeolite A is an aluminosilicate microporous material in which sodium ions can easily be exchanged. The principal building units are sodalite cages connected by four-membered rings, giving a cubic 3D network. It is an open zeolite with a large central cage.
[l] Zeolite F is a small-pore zeolite consisting of 2 different types of 8-membered ring channels systems with EDI-type framework.

Sulphate-rich aqueous waste

Sulphates present in RAW promote microstructural changes in Portland cement-based materials. Expansion and cracking due to the sulphate attack may cause a release of radionuclides[108]. Asano et al.[109] proposed an alternative two-step solidification process in which the aqueous sodium sulphate is converted into insoluble barium sulfate by mixing with barium hydroxide octahydrate. Later, the solution containing NaOH and $BaSO_4$ is mixed with an aluminosilicate source to solidify:

$$Ba(OH)_2(aq) + Na_2SO_4\ (aq) \rightarrow BaSO_4(s) + 2NaOH(aq)$$

The sulphates were stabilized as a precipitate of $BaSO_4$ which is also beneficial for the radiation shielding properties of the AAM due to the high atomic number of barium. A similar one-step process was proposed by Mobasher et al.[110] were all the components: Na_2SO_4, $Ba(OH)_2$ and a precursor material as blast furnace slag (BFS) are all mixed in one step. The direct addition of $Ba(OH)_2$ to the BFS promotes the reactivity and results in more C-S-H products. Also, ettringite and barium carbonate are formed instead of the hydrotalcite phase which was the main reaction product in the two-step process. Both processes could successfully immobilize the aqueous sulphate waste[32,109,110].

3.2. Zeolites

Radioactive $^{137}Cs^+$ and $^{90}Sr^{2+}$ are always present in the cooling water of nuclear reactors. The removal of these radionuclides is executed by using natural zeolites as clinoptilolite, which has a high exchange capacity for both the ions[111]. After usage, clinoptilolite is classified as a RAW material and need to be encapsulated. The encapsulation of a zeolite contaminated with cesium and/or strontium by alkali-activation technology was investigated by Kuenzel et al.[72]. Sodium and potassium metakaolin based geopolymers were used. Due to the high pH of the activating solution the clinoptilolite partly dissolves. The same was observed by Ke et al.[112]. The released aluminates and silicates take part in the alkali-activation reaction with incorporation of Cs and Sr is the geopolymer binder phase. Dissolution of zeolites is observed at a pH above 11[72]. The dissolution decreases over time due to the consumption of hydroxides during the dissolution process. The dissolved species lead to the formation of an interfacial transition zone of ± 0.15 mm, between the geopolymer matrix and the encapsulated zeolite, in which the chemical composition gradually evolves from one phase to another[72]. The dissolved species of the zeolite are thus directly incorporated in the geopolymer network. This behavior is however only valid for zeolites with high Si/Al molar ratio (>3.00)[113].

The dissolution of zeolites depends on the cation type used in the alkali-activator. Ke et al.[112] found higher dissolution of zeolites using potassium instead of sodium as cation. A clear transition zone which grows into the zeolite particle was observed for the potassium based geopolymers. A possible explanation is the lower viscosity of a potassium silicate solution which can therefore better penetrate the porous network of the zeolite.

Kuenzel et al.[72] concluded that Na-geopolymers tend to immobilize the cesium resulting from zeolite encapsulation better than K-geopolymers, with no detectable leaching of cesium for Na-geopolymers. The cesium replaces the sodium in the geopolymers since they are preferentially bound to aluminate phases. Cs^+ ions act as a weak Lewis acid and aluminates are weak Lewis bases. The reaction of Cs^+ with aluminate is favored, followed by K^+ and Na^+. No changes in the geopolymer network due to the incorporation of cesium were observed. The immobilization of Sr^{2+} in Na-geopolymers is limited. Strontium is only for a small fraction immobilized as a charge balancing ion[72,114]. 0.4 mol of Sr per mole of Al can be incorporated.

Most strontium will precipitate as a hydroxide or carbonate, especially at Sr/Al molar ratios higher than 0.4. No evidence was found to prove that Sr^{2+} could be incorporated in de C(-A)-S-H gel as a Ca^{2+} replacer. Elakneswaran et al.[114] found that Sr^{2+} can also be electrostatically adsorbed to the geopolymer surface.

Xu et al. [84] encapsulated exhausted type A zeolites with ^{90}Sr in metakaolin based geopolymers. These types of zeolites have a low Si/Al content and are considered not to dissolve in alkaline media. It was thus not a surprise that most of the strontium remains in the zeolites after encapsulation. Leaching experiments were executed and indicate that the geopolymer matrices immobilize the radionuclides better than the cementitious matrices in every media, from acid (pH = 1) to neutral (pH = 7). The initial process in the leaching behavior, (i) surface wash-off, was similar for both cementitious and geopolymer matrices. In a later stadium, Sr^{2+} ions from deeper layers will diffuse to the surface and leach out. In the (ii) diffusion stage, geopolymers performed better compared to OPC binders mainly due to their lower permeability. Geopolymers also have a better acid resistance since in acid media, Ca-rich phases easily dissolve, causing decalcification of the binder system in cementitious materials[115,116].

3.3. Aluminum containing waste

Due to the high pH of OPC based systems, they cannot be used to encapsulate RAW streams containing aluminum metal. This is the case for Magnox swarf with trace levels of Al metal from the Magnox reactors in the UK, Italy and Japan. In these reactors, a Mg/Al alloy was used as a fuel rod cladding material. The aluminum however easily corrodes at a pH above 11[117], giving rise to the production of hydrogen gas. Since the pH of geopolymers can be adapted by the selection of metakaolin and sodium silicate solution, they form an interesting alternative. Kuenzel et al.[117] showed that a low pH geopolymer system can be produced. However, lowering the pH of the activation solution leads to a lower strength and a longer setting time of the material. A geopolymer with a pH of 12.5 was produced, limiting but not avoiding the Al corrosion. Corrosion of the Al metal is retarded since hydroxide ions close to the metal surface are consumed by Al to form $Al(OH)^-_4$. Dissolved aluminum can take part in the geopolymerisation reaction and form alumina-silicate monomers. There is also a competition with the metakaolin, which uses hydroxides to dissolve, causing the pH to decrease in time. Moreover, at the interface of the metal with the binder, a layer of bayerite and gibbsite ($Al(OH_3)$) is formed, protecting the underlaying metal from further corrosion[117].

3.4. Mg alloys

The dismantling of gas cooled reactors as e.g. UNGG[m] reactors in France generates large volumes of a specific metallic waste. The waste consists of graphite tubes containing a metallic uranium rod cladded by a magnesium alloy. Before reprocessing the metallic uranium, assemblies have to be detached and thus a waste from graphite and a Mg-Zr alloy is produced. In Great Britain, the dismantling of the MAGNOX[n] reactors leads to a similar Mg-Al alloy RAW[118]. When incorporating these materials in a matrix of OPC, hydrogen gas generation is produced as a result of the formation of $Mg(OH)_2$. Cannes et al.[119] however suggest that it's also oxidized by another oxidant than water. The H_2 production is related to the corrosion of magnesium and is caused by anodic hydrogen evolution[120]. Monovalent magnesium ions will undergo an anodic dissolution in aqueous media and produce hydrogen gas.

[m] UNGG: Uranium Naturel Graphite Gaz (A UNGG reactor is graphite moderated, carbon dioxide cooled and fueled with natural aranium)

[n] MAGNOX: A MAGNOX reactor is graphite moderated, carbon dioxide cooled and fueled with natural aranium with magnesium-aluminium cladded fuel rods.

$$Mg^{+} + 2H_2O \rightarrow Mg^{2+} + 2OH^{-} + H_2$$

Alkali activated materials are interesting materials for the immobilization of Mg-Zr alloys since they only have a low amount of Ca[121]. Therefore, NaF can be added to the binder formulation in order to decrease Mg corrosion and the related dihydrogen production. A passivation layer of MgF_2, $NaMgF_3$, Na_2SiF_6 and Na_3AlF_6 can be formed[23,122]. In calcium rich binders as for OPC binders, NaF cannot be added since it would precipitate as CaF_2 and would deteriorate the mechanical properties. The high pH of Portland cement, however induces the formation of a $Mg(OH)_2$ layer on the surface of the metal which protects the underlying metal for further corrosion (Figure 12). This protection layer can unfortunately be destabilized by species from cement. SO_4^{2-} ions for example, from the dissolution of gypsum, destabilizes the protection layer. Geopolymers have the advantage to have a high amount of silicates which can form a layer of $MgSiO_4$ on the surface of the magnesium preventing it from corroding[23,122]. Corrosion rates (P_H) were studied by Lambertin et al.[123], and they found the following ranking:

$$P_{H\text{-}OPC} >> P_{H\text{-}GEO} > P_{H\text{-}OPC+[NAF]=1.25\ M} \sim P_{H\text{-}GEO+[NAF]=1.5\ M}$$

The corrosion rate is highly dependent on the pH[124]. The lowest corrosion rates were reported at pH values higher than 12. In this case, the high amount of OH^- favors the nucleation and formation of a thin homogeneous layer on the surface. The highest corrosion rate was observed for pH values between 10.45 and 11.44. The lower concentration of OH^- favors the growth of existing crystals instead of the formation of new sites. In this case a heterogeneous layer is formed, which is less protective[124].

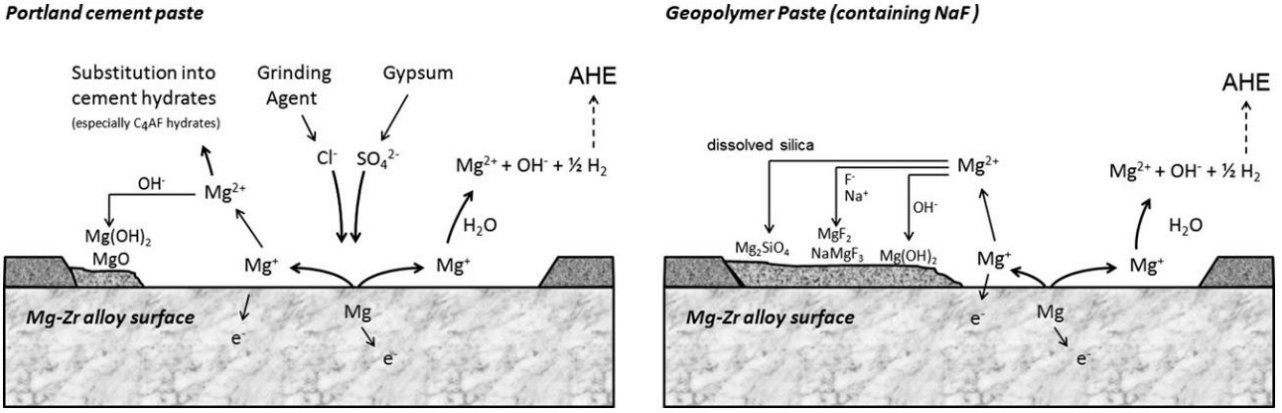

Figure 12: Model of magnesium alloy anodic corrosion behavior in Portland cement paste (left) and geopolymer paste (right)- AHE indicates the Anodic Hydrogen Evolution [122].

Rooses et al.[23,122] used metakaolin based geopolymers to immobilize Mg-Zr alloys. The galvanic corrosion of the geopolymers was low compared to the corrosion in Portland cement. Moreover, sodium based geopolymers seemed to be more suitable for Mg alloy encapsulation than potassium based geopolymers from the point of hydrogen production[23,119]. As a conclusion, Rooses et al.[23] defined a reference formulation of a geopolymer for Mg-Zr encapsulation: "The reference formulation of the geopolymer consists of a waterglass alkali solution with 386 g. L^{-1} of NaOH, 347 g. L^{-1} of SiO_2, 1.25 mol. L^{-1} (52 g. L^{-1}) of NaF, mixed with metakaolin and silicate sand with respective water/metakaolin and sand/metakaolin ratios of 0.78 and 1.5. This formulation is called "Na-Geo" and is patented by Lambertin et al.[125] Rifai et al.[118] succeeded in encapsulating Mg alloys in a NaOH activated ground granulated blast furnace slag and also observed a low hydrogen gas yield. However, a known problem for AAMs that needs to be solved, is the large autogenous and drying shrinkage.

Another problem is the possible contamination of the Mg-waste with uranium. For a high pH (>10) uranium is oxidized to UO_2, UO_3 or U_3O_8. It was found that the presence of fluoride ions promotes the corrosion of uranium. The fluoride ions diffuse to the oxides layer and cause desquamation resulting in crack formation and H_2 production[119]. If fluoride is absent, no corrosion of uranium was observed due to the protective oxides layer.

Another technique for immobilizing metals with zero oxidation is described in the patent of Lambertin et al.[126] in which the metal is dissolved in a molten hydroxide salt (e.g. KOH, NaOH or $Pb(OH)_2$). Next an alkaline solution is created by dissolving the melt in water. This solution can then be used for alkali-activation of an alumino-silicate source.

3.5. An example

In 2013, the first AAM was introduced successfully for nuclear waste encapsulation. SIAL®,[127] is a metakaolin based geopolymer developed and used for the immobilization of a highly contaminated sludge for which conventional methods using cementation or bitumen treatment could not be used due to the presence of radionuclides, including ^{137}Cs which easily leaches out. This material can incorporate four times as much waste as a traditional cement matrix and the encapsulation process takes less time. The material has a higher mechanical strength, lower leachability for radionuclides, low fire risk, high radiation stability and good physical stability in the presence of frost and water[127,128]. However, a decrease in compressive strength ranging from 16 to 39 % was found when this material was irradiated to a total dose of 1.027 MGy using a ^{60}Co source with a dose rate of 2.5 kGy. h^{-1} [128]. The SIAL matrix was approved to be used as a waste package for sludges and resins by Slovak and Czech Nuclear Regulatory Authorities.

4. Conclusions and Outlook

Alternatives to the commonly used ordinary Portland cement (OPC) matrices are increasingly being studied for application in the immobilization of toxic and radioactive materials. Alkali Activated Materials (AAMs) are one of the alternatives currently studied intensively due to their potential utilization as a high performance, environmental friendly and sustainable alternative to Portland cement. AAMs are high chemical and temperature resistant. Moreover, they can be designed to have a low water content and thus generate less radiolytic hydrogen gas compared to OPC based matrices. It is however not only the water content which defines the H_2 yield, but also the pore sizes and the diffusion coefficient of the material under consideration. AAMs also have a lower calcium content than ordinary OPC based mortars which enables the addition of fluorine to reduce the H_2 production for Mg-containing wastes and limits the formation of the long living ^{41}Ca radionuclide due to neutron activation. The challenge for future AAM designs lies in the elimination of the elements which can form long-lived radionuclides as a result of neutron activation (e.g. Cl, Th, Ca, Ni, U, Pu, C, K, Zr).

AAMs based on slags show high potential for use as gamma shielding material. High linear attenuation coefficients can be obtained only using cheap slags and avoiding expensive aggregates currently used to produce high density concretes. Fayalite slag based AAMs were proven to have a similar gamma shielding capacity to basalt-magnetite concretes. Also for neutron shielding, AAMs form an interesting opportunity since boron can be incorporated in the matrix as a substituent of aluminum. Moreover, AAMs lose less water in time in comparison to fresh OPC samples what creates the possibility to easily design AAMs with better neutron shielding capacities compared to aged concrete.

AAMs in general seem to be more stable when subjected to ionizing radiation compared to OPC based matrices. However, when irradiated with gamma rays, changes in pore size distribution and compressive strength could be observed. In an alpha particle irradiation field, crystallization effects can occur also influencing the pore size distribution.

The absence of portlandite, the low water content, the high alkalinity and the high temperature resistance makes AAMs interesting candidates for the conditioning of certain radioactive waste streams. Depending on the specific waste stream and the chosen AAM design, a different immobilization mechanism may be of importance. Ions as Cs^+ and Sr^{2+} can be incorporated in the AAM-gel or can be trapped in the self-generated or introduced zeolite structures in the AAM. Radioactive zeolite structures can also directly be incorporated in the AAM matrix. Due the high pH, zeolites may partially dissolve with the formation of a interfacial transition zone between the AAM matrix and the encapsulated zeolite. Also precipitation of several elements as an hydroxide is promoted due to the high alkalinity of AAMs. The conditioning of Al containing waste is still a challenge, since Al metal easily corrodes at a pH above 11. The development of low pH AAMs can be of interest in this field.

Models describing the irradiation effect and the relations between molecular-level chemical and physical characteristics and macroscopically measurable performances are missing for alkali activated materials. It remains a future challenge to predict in a reliable way the durability properties of tailor-made alkali activated materials when they are used in nuclear applications.

References

1. Provis, J. L. & Van Deventer, J. S. J. *Alkali-Activated Materials- State-of-the-Art Report, RILEM TC 224-AAM*. **13**, (Springer, 2014).

2. Davidovits, J. Geopolymer, Green Chemistry and Sustainable Development Solutions. in *Proceedings of the World Congress Geopolymer 2005* (ed. Davidovits, J.) 236 (Institut Géopolymère, 2005).

3. Krivenko, P. Why alkaline activation - 60 years of the theory and practice of alkali-activated materials. *J. Ceram. Sci. Technol.* **8**, 323–333 (2017).

4. Duxson, P. *et al.* Geopolymer technology : the current state of the art. *J Mater Sci* **42**, 2917–2933 (2007).

5. J. L. Provis and J. S. J. van Deventer, *Geopolymers: structure, processing, properties and industrial applications*. (Woodhead Publishing Limited, 2009). doi:10.1533/9781845696382.1.37

6. Barbosa, V. F. ., MacKenzie, K. J. . & Thaumaturgo, C. Synthesis and characterisation of materials based on inorganic polymers of alumina and silica: sodium polysialate polymers. *Int. J. Inorg. Mater.* **2**, 309–317 (2000).

7. Davidovits, J. Geopolymers - Inorganic polymeric - new materials. *J. Therm. Anal.* **37**, 1633–1656 (1991).

8. Peys, A. *et al.* Molecular structure of CaO – FeOx – SiO2 glassy slags and resultant inorganic polymer binders. *J. Am. Ceram. Soc.* **101**, 5846–5857 (2018).

9. Croymans-Plaghki, T. Valorization of Fe-rich industrial by-products in construction materials: a radiological assessment. (UHasselt, 2018).

10. Provis, J. L. & Bernal, S. A. Geopolymers and Related Alkali-Activated Materials. *Annu. Rev. Mater. Res.* **44**, 299–327 (2014).

11. Ukritnukun, S., Sorrell, C. C., Gregg, D., Vance, E. R. & Koshy, P. Potential Use of Ambient-Cured Geopolymers for Intermediate Level Nuclear Waste Storage. *MRS Adv.* **3**, 1123–1131 (2018).

12. Van Jaarsveld, J. G. S., Van Deventer, J. S. J. & Lorenzen, L. Potential use of geopolymeric materials to immobilize toxic metals: Part I. Theory and applications. *Miner. Eng.* **10**, 659–669 (1997).

13. Vance, E. R. & Perera, D. S. Geopolymers for nuclear waste immobilisation. in *Geopolymers: Structure, Processing, Properties and Industrial Applications* (eds. L. Provis, J. & S.J. van Denveter, J.) 403–422 (Woodhead Publishing, 2009). doi:10.1533/9781845696382.3.401

14. Vance, E. R. & Perera, D. S. Development of geopolymers for nuclear waste immobilisation. in *Handbook of Advanced Radioactive Waste Conditioning Technologies* 207–229 (Woodhead Publishing Limited, 2011).

15. Chupin, F., Dannoux-papin, A., Ravache, Y. N. & D'Espinose de Lacaillerie, J.-B. Water content and porosity effect on hydrogen radiolytic yields of geopolymers. *J. Nucl. Mater.* **494**, 138–146 (2017).

16. Vandevenne, N. *et al.* Incorporating Cs and Sr into blast furnace slag inorganic polymers and their effect on matrix properties. *J. Nucl. Mater.* **503**, 1–12 (2018).

17. Shi, C. & Fernández-Jiménez, A. Stabilization/solidification of hazardous and radioactive wastes with alkali-activated cements. *J. Hazard. Mater.* **137**, 1656–1663 (2006).

18. Duan, P., Yan, C., Zhou, W., Luo, W. & Shen, C. An investigation of the microstructure and durability of a fluidized bed fly ash–metakaolin geopolymer after heat and acid exposure. *Mater. Des.* **74**, 125–137 (2015).

19. Provis, J. L. Geopolymers and other alkali activated materials: why, how, and what? *Mater. Struct.* **47**, 11–25 (2014).

20. International Atomic Energy Agency. *The Behaviours of Cementitious Materials in Long Term Storage and Disposal of Radioactive Waste : Results of a Coordinated Research Project.* (2013).

21. Drace, Z. & Ojovan, M. I. Cementitious materials for radioactive waste management within IAEA Coordinated Research Project. in *Proceedings of the International Conference on Radioactive Waste Management and Environmental Remediation, ICEM* 5–13 (IAEA, 2011). doi:10.1115/ICEM2011-59021

22. B. Florence, C. Cau-dit-Coumes, F. Frizon, and S. Lorente, *Cement-Based Materials for Nuclear Waste Storage*. (Springer, 2013). doi:10.1007/978-1-4614-3445-0

23. Rooses, A. *et al.* Encapsulation of Mg-Zr alloy in metakaolin-based geopolymer. *Appl. Clay Sci.* **73**, 86–92 (2013).

24. Mobasher, N., Bernal, S. A., Kinoshita, H. & Sharrad, C. A. Gamma irradiation resistance of an early age slag-blended cement matrix for nuclear waste encapsulation. *J. Mater. Res.* **30**, 1563–1571 (2015).

25. Kaplan, M. F. *Concrete radiation shielding : nuclear physics, concrete properties, design and construction*. (Longman Scientific and Technical, 1989).

26. Machiels, L., Arnout, L., Jones, P. T., Blanpain, B. & Pontikes, Y. Inorganic polymer cement from fe-silicate glasses: Varying the activating solution to glass ratio. *Waste and Biomass Valorization* **5**, 411–428 (2014).

27. Simon, S., Gluth, G. J. G., Banerjee, D. & Pontikes, Y. The fate of iron during the alkali-activation of synthetic (CaO-) FeO x -SiO2 slags : An Fe K-edge XANES study. *J. Am. Ceram. Soc.* **101**, 2107–2118 (2018).

28. Lemougna, P. N., Mackenzie, K. J. D., Jameson, G. N. L. & Chinje, H. R. U. F. The role of iron in the formation of inorganic polymers (geopolymers) from volcanic ash : a 57Fe Mössbauer spectroscopy study. *J. Mater. Sci.* **48**, 5280–5286 (2013).

29. Peys, A. *et al.* Inorganic Polymers From CaO-FeOx-SiO2 Slag: The Start of Oxidation of Fe and the Formation of a Mixed Valence Binder. *Front. Mater.* **6**, 1–10 (2019).

30. Mohammed, K. S., Azeez, A. B., Bakri, A. M. M. A., Hussin, K. & Azmi, B. R. The Effect of Barite Content on Anti Radiation Properties of Geopolymer Fly Ash Concrete Incorporated Natural Rock Ores of Hematite. *J. Sci. Res.* **3**, 1818–1827 (2012).

31. Shalbi, S. M. *et al.* Effect of fly ash geopolymer with 15 % barium Sulphate as a design shielding box on radiation attenuation using GafchramicXR-QA2 film dosimetry. *J. Eng.* **7**, 13–17 (2017).

32. Mobasher, N., Bernal, S. A., Kinoshita, H. & Provis, J. L. Gamma irradiation resistance of early age Ba(OH)2Na2SO4-slag cementitious grouts. *J. Nucl. Mater.* **482**, 266–277 (2016).

33. Williams, R. P. & van Riessen, A. Development of alkali activated borosilicate inorganic polymers (AABSIP). *J. Eur. Ceram. Soc.* **31**, 1513–1516 (2011).

34. Montes, C. *et al.* Evaluation of lunar regolith geopolymer binder as a radioactive shielding material for space exploration applications. *Adv. Sp. Res.* **56**, 1212–1221 (2015).

35. Fillmore, D. L. *Literature Review of the Effects of Radiation and Temperature on the Aging of Concrete - Prepared for the Central Research Institute of Electric Power Institute - INEEL/EXT-04-02319*. (Idaho National Engineering and Environmental Laboratory, 2004).

36. Rosseel, T. M. *et al.* Review of the Current State of Knowledge on the Effects of Radiation on Concrete. *J. Adv. Concr. Technol.* **14**, 368–383 (2016).

37. Vodák, F., Vydra, V., Trtík, K. & Kapičková, O. Effect of gamma irradiation on properties of hardened cement paste. *Mater. Struct.* **44**, 101–107 (2010).

38. Bouniol, P. & Bjergbakke, E. A comprehensive model to describe radiolytic processes in cement medium. *J. Nucl. Mater.* **372**, 1–15 (2008).

39. Le Caër, S. Water Radiolysis: Influence of Oxide Surfaces on H2 Production under Ionizing Radiation. *Water* **3**, 235–253 (2011).

40. Bjergbakke, E., Sehested, K., Lang Rasmussen, O. & Christensen, H. *Input files for computer simulation of water radiolysis*. (1984).

41. Vodák, F., Vydra, V., Trtík, K. & Kapičková, O. Effect of gamma irradiation on properties of hardened cement paste. *Mater. Struct.* **44**, 101–107 (2011).

42. Li, W. *et al.* Effect of vacuum dehydration on gel structure and properties of metakaolin-based geopolymers. *Ceram. Int.* **43**, 14340–14346 (2017).

43. Duxson, P. *et al.* Understanding the relationship between geopolymer composition, microstructure and mechanical properties. *Colloids Surfaces A Physicochem. Eng. Asp.* **269**, 47–58 (2005).

44. Lambertin, D. *et al.* Influence of gamma ray irradiation on metakaolin based sodium geopolymer. *J. Nucl. Mater.* **443**, 311–315 (2013).

45. Chupin, F. Caractérisation de l 'effet des irradiations sur les géopolymères. (Université Pierre et Marie Curie, 2015).

46. Cantarel, V., Arisaka, M. & Yamagishi, I. On the hydrogen production of geopolymer wasteforms under irradiation. *J. Am. Ceram. Soc.* 1–11 (2019). doi:10.1111/jace.16642

47. Bykov, G. L., Gordeev, A. V., Yurik, T. K. & Ershov, B. G. Gas formation upon γ-irradiation of cement material. *High Energy Chem.* **42**, 211–214 (2008).

48. Leay, L., Potts, A. & Donoclift, T. Geopolymers from fly ash and their gamma irradiation. *Mater. Lett.* **227**, 240–242 (2018).

49. Bjergbakke, E., Sehested, K., Lang Rasmussen, O. & Christensen, H. *Input files for computer simulation of water radiolysis*. (1984).

50. Boher, C., Martin, I., Lorente, S. & Frizon, F. Experimental investigation of gas diffusion through monomodal materials. Application to geopolymers and Vycor® glasses. *Microporous Mesoporous Mater.* **184**, 28–36 (2014).

51. Le Caër, S. *et al.* Radiolysis of confined water: Hydrogen production at a high dose rate. *ChemPhysChem* **6**, 2585–2596 (2005).

52. Rotureau, P., Renault, J. P., Lebeau, B., Patarin, J. & Mialocq, J. C. Radiolysis of confined water: Molecular hydrogen formation. *ChemPhysChem* **6**, 1316–1323 (2005).

53. Mast, B. *et al.* The effect of gamma radiation on the mechanical and microstructural properties of Fe-rich inorganic polymers. *J. Nucl. Mater.* **521**, (2019).

54. Mubasher, T. A., Leay, L., Hayes, M. & Butcher, E. Evaluation of Novel Geopolymer-based Materials for Nuclear Waste Treatment. in *NUWCEM - 3rd International Symposium on Cement-Based Materials for Nuclear Wastes* 1–5 (CEA, 2018).

55. Spinks, J. W. T. & Woods, R. J. An introduction to radiation chemistry. *J. Chem. eduction* **55**, (1978).

56. Deng, N. *et al.* Effects of gamma-ray irradiation on leaching of simulated 133Cs+ radionuclides from geopolymer wasteforms. *J. Nucl. Mater.* **459**, 270–275 (2015).

57. Piao, F., Oldham, W. G. & Haller, E. E. Mechanism of radiation-induced compaction in vitreous silica. *J. Non. Cryst. Solids* **276**, 61–71 (2000).

58. Sandhu, A. K., Singh, S. & Pandey, O. P. Gamma ray induced modifications of quaternary silicate glasses. *J. Phys. D. Appl. Phys.* **41**, 165402–165408 (2008).

59. Arbel-Haddad, M. *et al.* The Effect of Gamma Irradiation on the Structure and Binding Properties of Amorphous and Partially- Crystalline Geopolymer Matrices. in *NUWCEM -Cement-based Materials for Nuclear Wastes* (2018).

60. Craeye, B., De Schutter, G., Vuye, C. & Gerardy, I. Cement-waste interactions: Hardening self-compacting mortar exposed to gamma radiation. *Prog. Nucl. Energy* **83**, 212–219 (2015).

61. Maruyama, I. *et al.* Impact of gamma-ray irradiation on hardened white Portland cement pastes exposed to atmosphere. *Cem. Concr. Res.* **108**, 59–71 (2018).

62. Mast, B. *et al.* The effect of gamma radiation on the mechanical and microstructural properties of Fe-rich inorganic polymers. *J. Nucl. Mater.* **521**, 126–136 (2019).

63. Azmi, M., Hamid, A. & Kamil, N. pH-dependent magnetic phase transition of iron oxide nanoparticles synthesized by gamma-radiation reduction method. *J. Radioanal Nucl Chem* **301**, 399–407 (2014).

64. Takeda, H., Hashimoto, S., Matsui, H., Honda, S. & Iwamoto, Y. Rapid fabrication of highly dense geopolymers using a warm press method and their ability to absorb neutron irradiation. *Constr. Build. Mater.* **50**, 82–86 (2014).

65. Bylkin, B. K., Engovatov, I. A., Kozhevnikov, A. N. & Sinyushin, D. K. On the necessity and the role of descriptors of neutron activated structural and shielding materials of nuclear installations for future decommissioning. *Nucl. Energy Technol.* **4**, 257–262 (2018).

66. Bylkin, B. K., Kozhevnikov, A. N., Engovatov, I. A. & Sinyushin, D. K. Radioactivity Category

Determination for Radiation-Protection Concrete in Nuclear Facilities Undergoing Decommissioning. *At. Energy* **121**, 383–387 (2017).

67. Evans, J. P. *et al. Long-Lived Activation Products in Reactor Materials*. (1984).

68. Bai, Y., Collier, N. C., Milestone, N. B. & Yang, C. H. The potential for using slags activated with near neutral salts as immobilisation matrices for nuclear wastes containing reactive metals. *J. Nucl. Mater.* **413**, 183–192 (2011).

69. Dimas, D. D., Giannopoulou, I. P. & Panias, D. Utilization of Alumina Red Mud for Synthesis of Inorganic Polymeric Materials. *Miner. Process. Extr. Metall. Rev.* **30**, 211–239 (2009).

70. Xu, H. & Van Deventer, J. S. J. The geopolymerisation of alumino-silicate minerals. *Int. J. Miner. Process.* **59**, 247–266 (2000).

71. Khalil, M. Y. & Merz, E. Immobilization of intermediate-level wastes in geopolymers. *J. Nucl. Mater.* **211**, 141–148 (1994).

72. Kuenzel, C. *et al.* Encapsulation of Cs/Sr contaminated clinoptilolite in geopolymers produced from metakaolin. *J. Nucl. Mater.* **466**, 94–99 (2015).

73. Peng, X., Xu, Y., Xu, Z., Wu, D. & Li, D. Effect of simulated radionuclide strontium on geopolymerization process. *procedia Environ. Sci.* **31**, 325–329 (2016).

74. Xiaodong, S., Sheng, Y., Xuequan, W. & Mingshu, T. Immobilization of Simulated High Level Wastes Into Waste Form. *Cem. Concr. Res.* **24**, 133–138 (1994).

75. Goñi, S., Guerrero, A. & Lorenzo, M. P. Efficiency of fly ash belite cement and zeolite matrices for immobilizing cesium. *J. Hazard. Mater.* **137**, 1608–1617 (2006).

76. Blackford, M. G., Hanna, J. V., Pike, K. J., Vance, E. R. & Perera, D. S. Transmission Electron Microscopy and Nuclear Magnetic Resonance Studies of Geopolymers for Radioactive Waste Immobilization. *J. Am. Ceram. Soc.* **90**, 1193–1199 (2007).

77. Provis, J. L., Walls, P. . A. & Van Deventer, J. S. J. Geopolymerisation kinetics. 3. Effects of Cs and Sr salts. *Chem. Eng. Sci.* **63**, 4480–4489 (2008).

78. Aly, Z. *et al.* Aqueous leachability of metakaolin-based geopolymers with molar ratios of Si / Al = 1 . 5 – 4. *J. Nucl. Mater.* **378**, 172–179 (2008).

79. Chlique, C., Lambertin, D., Antonucci, P., Frizon, F. & Deniard, P. XRD Analysis of the Role of Cesium in Sodium-Based Geopolymer. *J. Am. Ceram. Soc.* **98**, 1308–1313 (2015).

80. Shiota, K. *et al.* Stabilization of cesium in alkali-activated municipal solid waste incineration fly ash and a pyrophyllite-based system. *Chemosphere* **187**, 188–195 (2017).

81. Qian, G., Sun, D. D. & Tay, J. H. New aluminium-rich alkali slag matrix with clay minerals for immobilizing simulated radioactive Sr and Cs waste. *J. Nucl. Mater.* **299**, 199–204 (2001).

82. Brough, A. R. *et al.* Adiabatically cured , alkali-activated cement-based wasteforms containing high levels of fly ash Formation of zeolites and Al-substituted C-S-H. *Cem. Concr. Res.* **31**, 1437–1447 (2001).

83. Jang, J. G., Park, S. M. & Lee, H. K. Cesium and Strontium Retentions Governed by Aluminosilicate Gel in Alkali-Activated Cements. *Materials (Basel).* **10**, 1–13 (2017).

84. Xu, Z. *et al.* Immobilization of strontium-loaded zeolite A by metakaolin based- geopolymer. *Ceram. Int.* **43**, 4434–4439 (2017).

85. Guangren, Q., Yuxiang, L., Facheng, Y. & Rongming, S. Improvement of metakaolin on radioactive Sr and Cs immobilization of alkali-activated slag matrix. *J. Hazard. Mater.* **92**, 289–300 (2002).

86. Xuequan, W., Sheng, Y., Xiadong, S. & Mingshu, T. Alkali-activated slag cement based radioactive waste forms. *Cem. Concr. Res.* **21**, 16–20 (1991).

87. Jang, J. G., Park, S. M. & Lee, H. K. Physical barrier effect of geopolymeric waste form on diffusivity of cesium and strontium. *J. Hazard. Mater.* **318**, 339–346 (2016).

88. Sora, I. N., R. Pelosato, Botta, D. & G. Dotelli. Chemistry and microstructure of cement pastes admixed with organic liquids. *J. Eur. Ceram. Soc.* **22**, 1463–1473 (2002).

89. Pollard, S. J. T., Montgomery, D. M., Sollars, C. J. & Perry, R. Organic compounds in the cement-based stabilisation/ solidification of hazardous mixed wastes-Mechanistic and process considerations. *J. Hazard. Mater.* **28**, 313–327 (1991).

90. International Atomic Energy Agency. *Treatment and conditioning of radioactive organic liquids*. (1992).

91. Cantarel, V. *et al.* Solidification/stabilisation of liquid oil waste in metakaolin-based geopolymer. *J. Nucl. Mater.* **464**, 16–19 (2015).

92. Lambertin, D., Rooses, A. & Frizon, F. Process for preparing a composite material from an organic liquid and resulting material -AU 2013320269 B2. (2017).

93. Cantarel, V. Etude de la synthèse de composites liquides organiques/geopolymère en vue du conditionnement de déchets nucléaires. (Université Blaise Pascal, 2016).

94. Cantarel, V. *et al.* Geopolymer assembly by emulsion templating : Emulsion stability and hardening mechanisms. *Ceram. Int.* **44**, 10558–10568 (2018).

95. Davy, C. A., Hauss, G., Planel, B. & Lambertin, D. 3D structure of oil droplets in hardened geopolymer emulsions. *J. Am. Ceram. Soc.* **102**, 949–954 (2018).

96. Wang, J. *et al.* Preparation of Alkali-Activated Slag-Fly Ash-Metakaolin Hydroceramics for Immobilizing Simulated Sodium-Bearing Waste. *Am. Ceram. Soc.* **98**, 1393–1399 (2015).

97. Li, Z., Ohnuki, T. & Ikeda, K. Development of paper sludge ash-based geopolymer and application to treatment of hazardous water contaminated with radioisotopes. *Materials (Basel).* **9**, (2016).

98. Gallagher, S. A. & McCarthy, G. J. Preparation and X-ray characterization of pollucite (CsAlSi2O6). *J. Inorg. Nucl. Chem.* **43**, 1773–1777 (1981).

99. Arbel Haddad, M. *et al.* Formation of zeolites in metakaolin-based geopolymers and their potential application for Cs immobilization. *J. Nucl. Mater.* **493**, 168–179 (2017).

100. Liu, Q., Xu, H. & Navrotsky, A. Nitrate cancrinite: Synthesis, characterization, and determination of the enthalpy of formation. *Microporous Mesoporous Mater.* **87**, 146–152 (2005).

101. Ofer-Rozovsky, E. *et al.* Cesium immobilization in nitrate-bearing metakaolin-based geopolymers. *J. Nucl. Mater.* **514**, 247–254 (2019).

102. Arbel-Haddad, M. *et al.* Low-Silica Geopolymers As Candidate Matrices for Immobilization of Cesium Ions. in *NUWCEM - 3rd International Symposium on Cement-Based Materials for Nuclear Wastes* (2018).

103. Norby, P., Andersen, I. G. K., Andersen, E. K., Colella, C. & de'Gennaro, M. Synthesis and structure of lithium cesium and lithium thallium cancrinites. *Zeolites* **11**, 248–253 (1991).

104. Zhao, H., Deng, Y., Harsh, J. B., Flury, M. & Boyle, J. S. Alteration of kaolinite to Cancrinite and sodalite by simulated Hanford tank waste and its impact on cesium retention. *Clays Clay Miner.* **52**, 1–13 (2004).

105. Mon, J., Deng, Y., Flury, M. & Harsh, J. B. Cesium incorporation and diffusion in cancrinite, sodalite, zeolite, and allophane. *Microporous Mesoporous Mater.* **86**, 277–286 (2005).

106. Ofer-rozovsky, E., Arbel Haddad, M., Bar Nes, G. & Katz, A. The formation of crystalline phases in metakaolin-based geopolymers in the presence of sodium nitrate. *J. Mater. Sci.* **51**, 4795–4814 (2016).

107. Berger, S., Frizon, F. & Joussot-Dubien, C. Formulation of caesium based and caesium containing geopolymers. *Adv. Appl. Ceram.* **108**, 412–417 (2009).

108. Gollop, R. S. & Taylor, H. F. W. Microstructural and microanalytical studies of sulfate attack. IV. Reactions of a slag cement paste with sodium and magne- sium sulfate solutions. *Cem. Concr. Compos.* **26**, 1029–1044 (1996).

109. Asano, T., Kawasaki, T. & Higuchi, N. Feasibility Study of Solidification for Low-Level Liquid Waste Generated by Sulfuric Acid Elution Treatment of Spent Ion Exchange Resin. *J. Power Energy Syst.* **2**, 206–214 (2008).

110. Mobasher, N., Kinoshita, H., Bernal, S. A. & Sharrard, C. A. Ba(OH)2 – blast furnace slag composite binders for encapsulation of sulphate bearing nuclear waste. *Adv. Appl. Ceram.* **113**, 460–465

(2014).

111. Cappelletti, P. *et al.* Immobilization of Cs and Sr in aluminosilicate matrices derived from natural zeolites. *J. Nucl. Mater.* **414**, 451–457 (2011).

112. Ke, X., Bernal, S. A., Sato, T. & Provis, J. L. Encapsulation of strontium loaded ion-exchangers using metakaolin geopolymer : the influence of activator cations. in *NUWCEM - 3rd International Symposium on Cement-Based Materials for Nuclear Wastes* (2018).

113. Mimura, H. & Akiba, K. Adsorption behavior of cesium and strontium on synthetic zeolite P. *J. Nucl. Sci. Technol.* **30**, 436–443 (1993).

114. Elakneswaran, Y. *et al.* Interaction of strontium ions with metakaolin-based geopolymers. in *NUWCEM - 3rd International Symposium on Cement-Based Materials for Nuclear Wastes* (2018).

115. Bakharev, T. Resistance of geopolymer materials to acid attack. *Cem. Concr. Res.* **35**, 658–670 (2005).

116. Ariffin, M. A. M., Bhutta, M. A. R., Hussin, M. W., Mohd Tahir, M. & Aziah, N. Sulfuric acid resistance of blended ash geopolymer concrete. *Constr. Build. Mater.* **43**, 80–86 (2013).

117. Kuenzel, C. *et al.* Encapsulation of aluminium in geopolymers produced from metakaolin. *J. Nucl. Mater.* **447**, 208–214 (2014).

118. Rifai, F., Chartier, D., Stefan, L., Muzeau, B. & Darquennes, A. NUGG Waste Retrieval – development of an alkali-activated grout for graphite wastes mixed to reactive metals impurities. in *NUWCEM - 3rd International Symposium on Cement-Based Materials for Nuclear Wastes* 12 (2018).

119. Cannes, C. *et al.* Reactivity of Mg-Zr in Na-geopolymers , role of fluoride ions. in *Cement-based Materials for Nuclear Wastes* (2018).

120. Song, G. Recent progress in corrosion and protection of magnesium alloys. *Adv. Eng. Mater.* **7**, 563–586 (2005).

121. Chartier, D., Muzeau, B., Stefan, L., Sanchez-canet, J. & Monguillon, C. Magnesium alloys and graphite wastes encapsulated in cementitious materials : Reduction of galvanic corrosion using alkali hydroxide activated blast furnace slag. *J. Hazard. Mater.* **326**, 197–210 (2017).

122. Rooses, A., Lambertin, D., Chartier, D. & Frizon, F. Galvanic corrosion of Mg-Zr fuel cladding and steel immobilized in Portland cement and geopolymer at early ages. *J. Nucl. Mater.* **435**, 137–140 (2013).

123. Lambertin, D., Frizon, F. & Bart, F. Mg-Zr alloy behavior in basic solutions and immobilization in Portland cement and Na-geopolymer with sodium fluoride inhibitor. *Surf. Coatings Technol.* **206**, 4567–4573 (2012).

124. Barros, C. F., Muzeau, B., François, R. & Hostis, V. L'. Corrosion behavior of Mg-Zr alloy in alkaline solutions and in Na-geopolymer. in *NUWCEM - 3rd International Symposium on Cement-Based Materials for Nuclear Wastes* (2018).

125. LAMBERTIN, D., FRIZON, F., BLACHERE, A. & BART, F. Use of anticorrosion agents for conditioning magnesium metal, conditioning material thus obtained and preparation process. (2016). doi:10.1179/174367606X120142

126. Lambertin, D., Goettmann, F., Frizon, F. & Blachere, A. Process for dissolving a metal and implementation for conditioning said metal in a geopolymer FR3033444A1. (2016).

127. Lichvar, P., Rozloznik, M. & Sekely, S. *Behaviour of Aluminosilicate Inorganic Matrix SIAL During and After Solidification of Radioactive Sludge and Radioactive Spent Resins and Their Mixtures*. *Amec Nuclear Slovakia* (2013).

128. Majersky, D., Sekely, S., Zavodska, D. & Breza, M. Application of Inorganic SIAL Matrix and Movable Technology in Solidification of the TRU Sludges and Sludge / Resin Mixtures. in *WM'06 Conference* (2006).

Relevant Websites:

1. https://www.sreway.info/sredat/
2. http://www.nucleide.org/Laraweb/index.php
3. https://www.nist.gov/pml/xcom-photon-cross-sections-database.
4. https://www.geopolymer.org/
5. http://www.zeobond.com/
6. https://www.resourcefull.eu/